



# EASTLAND PORT MAINTENANCE DREDGING AND DISPOSAL PROJECT

Wave hindcast validation

Report prepared for Eastland Port

September 2017

MetOcean Solutions Ltd: Report P0331-05

July 2017

Report status

Version	Date	Status	Approved by
RevA	15/09/2017	Draft for internal review	Guedes/Monetti
RevB	19/09/2017	Draft for client review	Beamsley

It is the responsibility of the reader to verify the currency of the version number of this report.

The information, including the intellectual property, contained in this report is confidential and proprietary to MetOcean Solutions Ltd. It may be used by the persons to whom it is provided for the stated purpose for which it is provided, and must not be imparted to any third person without the prior written approval of MetOcean Solutions Ltd. MetOcean Solutions Ltd reserves all legal rights and remedies in relation to any infringement of its rights in respect of its confidential information.

## TABLE OF CONTENTS

1.	Introduction .....	7
2.	Model methods.....	10
2.1.	Bathymetry.....	10
2.2.	Model description .....	11
2.3.	Model Setup.....	11
2.4.	Post-processing .....	13
2.5.	Model uncertainty and validation methods.....	13
2.5.1.	Wind validation.....	13
2.5.2.	Wave validation.....	14
2.5.3.	Evaluation criteria .....	16
2.5.4.	Bias correction technique .....	16
3.	Results .....	18
3.1.	Quantitative validation .....	18
3.1.1.	Wind validation.....	18
3.1.2.	Wave validation.....	23
3.1.3.	Bias-corrected significant wave height .....	30
3.2.	Wave climate.....	32
4.	Summary.....	40
5.	References.....	41
	Appendix A. Measured and hindcast wind roses at Hicks Bay.....	42

**LIST OF FIGURES**

Figure 1.1 Maps showing the location of Poverty Bay (a and b), and Eastland Port (c) with the locations used in the present study. Both offshore disposal and shipping channel are indicated on top of the bathymetry in (d). ..... 8

Figure 1.2 Flow chart showing the numerical modelling process for the study. Red lines indicate hydrodynamics; blue indicates waves; green indicates wind and brown indicate bathymetry and yellow lines indicate sediments. .... 9

Figure 2.1 Map showing both the 500 x 500 m (top) and the 5 x 5 m (bottom) gridded bathymetries used to interpolate the water depth to the computational grid in SWAN. .... 10

Figure 2.2 Map showing the SWAN nested domains used to simulate the spectral transformation of the offshore wave climates to the nearshore zone. Information specific to each set-up is provided in Table 2.1. .... 12

Figure 2.3 Map showing the regional bathymetry of the continental shelf between Gisborne and East Cape. The white dots indicate the sites used to compare hindcast and measured wind data collected by weather stations. .... 14

Figure 2.4 Map showing the bathymetry over Poverty Bay. The orange dots indicate the location of the S4 current meter data used to validate the SWAN wave model. .... 15

Figure 3.1 Measured and modelled wind speed at 10 m between June and December 2002 (a), January and June 2003 (b). .... 20

Figure 3.2 Quantile-Quantile plot of the 10 m measured and model wind speeds at Gisborne Airport for the period 2000 – 2008. .... 21

Figure 3.3 Measured (top) and model (bottom) wind roses at Gisborne Airport for the period 2000 – 2008. Winds are reported in the “coming from” directional reference. .... 22

Figure 3.4. Model versus measured significant wave height  $H_s$  at the WB1 location during the year of 2012. Colours represent modelled (left) peak wave period  $T_p$  and (right) mean wave direction at the peak wave frequency ( $D_{pm}$ ) at an offshore reference site located at 178.3 E, 39.0 S. .... 24

Figure 3.5. Snapshot of wind velocities and mean sea level pressure during a low-pressure system on 28 June 2012. .... 24

Figure 3.6. Snapshot of significant wave height  $H_s$  during a low-pressure system on 19 May 2012. The rectangle limited by 180 – 183 E, 43 – 37 S shows the area over which  $H_s$  from the global wave model and satellite altimeters were collocated. .... 25

Figure 3.7. Time series of satellite altimeter and modelled significant wave height  $H_s$  collocated within 0.5° by 0.5° bins over the area delimited by 180 – 183 E, 43 – 37 S (see Figure 3.6) during 2012. Gray patches show identified periods influenced by extra-tropical cyclones (e.g. Figure 3.5) when waves were observed to be strongly under predicted at location WB1 (corresponding to the high-energy, long-period SE events shown in Figure 3.4). Note data from WB1 were scarce before May 2012 and the high-energy events earlier in the year shown here are not represented in Figure 3.4. .... 25

Figure 3.8. Scatter density (left) and scatter diagram (right) comparing satellite altimeter and modelled significant wave height  $H_s$  over the area limited

	by 180 –183 E, 43 – 37 S (see Figure 3.6) during 2012. Hot colours on the left indicate higher density of data-points. Red circles on the right show the quantile-quantile at the 0.01 percentile. ....	26
Figure 3.9.	Time series of measured and modelled significant wave height $H_s$ at site WB1 between 2007 – 2008. ....	26
Figure 3.10.	Scatter density (left) and scatter diagram (right) comparing measured and modelled significant wave height $H_s$ at WB1 site for years 2007–2008. Hot colours on the left indicate higher density of data-points. Red circles on the right show the quantile-quantile at the 0.01 percentile. ....	27
Figure 3.11.	Time series of measured and modelled significant wave height $H_s$ at site WB1 during 2014. ....	27
Figure 3.12.	Scatter density (left) and scatter diagram (right) comparing measured and modelled significant wave height $H_s$ at A1 site for 2014. Hot colours on the left indicate higher density of data-points. Red circles on the right show the quantile-quantile at the 0.01 percentile. ....	28
Figure 3.13.	Time series of measured and modelled peak wave period $T_p$ at site WB1 between 2007 – 2008. ....	28
Figure 3.14.	Scatter density (left) and scatter diagram (right) comparing measured and modelled peak wave period $T_p$ at WB1 site for years 2007–2008. Hot colours on the left indicate higher density of data-points. Red circles on the right show the quantile-quantile at the 0.01 percentile. ....	29
Figure 3.15.	Time series of measured and modelled peak wave period $T_p$ at site A1 during 2014. ....	29
Figure 3.16.	Scatter density (left) and scatter diagram (right) comparing measured and modelled significant peak wave period $T_p$ at A1 site during 2014. Hot colours on the left indicate higher density of data-points. Red circles on the right show the quantile-quantile at the 0.01 percentile. ....	29
Figure 3.17.	Time series of measured and bias-corrected, modelled significant wave height $H_s$ at site WB1 between 2007 – 2008. ....	31
Figure 3.18.	Scatter density (left) and scatter diagram (right) comparing measured and bias-corrected, modelled significant wave height $H_s$ at WB1 site for years 2007–2008. Hot colours on the left indicate higher density of data-points. Red circles on the right show the quantile-quantile at the 0.01 percentile. ....	31
Figure 3.19.	Time series of measured and bias-corrected, modelled significant wave $H_s$ height at site A1 during 2014. ....	32
Figure 3.20.	Scatter density (left) and scatter diagram (right) comparing measured and bias-corrected, modelled significant wave height $H_s$ at A1 site for 2014. Hot colours on the left indicate higher density of data-points. Red circles on the right show the quantile-quantile at the 0.01 percentile. ....	32
Figure 3.21.	Snapshot of significant wave height from the NZN 4 km SWAN parent domain on 29 July 2012, shown within the area delimited by the outer black rectangle. Model data from the 0.5° global wave model are shown outside of this area. Extension of Gisborne child nest is shown by the inner black rectangle. ....	33
Figure 3.22.	Snapshot of significant wave height from the Gisborne 500 m SWAN child domain on 29 July 2012, shown within the area delimited by the outer black rectangle. Model data from the 4 km NZN domain are	

	shown outside of this area. Extension of Poverty Bay child nest is shown by the inner black rectangle. ....	34
Figure 3.23.	Snapshot of significant wave height from the Poverty Bay 80 m SWAN child domain on 29 July 2012, shown within the area delimited by the outer black rectangle. Model data from the 500 m Gisborne domain are shown outside of this area. Extension of Eastland child nest is shown by the inner black rectangle. ....	34
Figure 3.24.	Boxplots extracted from time series of significant wave height at Sites WB1 (top) and A1 (bottom). The blue rectangles correspond to the 25 <sup>th</sup> – 75 <sup>th</sup> percentiles of the annual distributions. Red crosses and red lines indicate the annual median and mean, respectively. The grey dots correspond to the outliers based on the 95 <sup>th</sup> percentile threshold. ....	35
Figure 3.25.	Wave rose diagrams based on 10 year hindcast data (1996 – 2005) at Sites WB1 (top) and A1 (bottom). The direction follows the nautical “coming from” convention. ....	37
Figure 3.26.	Significant wave height ( $H_s$ ) time series at Sites WB1 (top) and A1 (bottom) including the extreme events detected from the Peaks over Threshold (POT) methodology. The dashed green line indicates the minimum threshold used for the detection of extreme events corresponding to the 95 <sup>th</sup> percentile level of the distribution. ....	38
Figure 3.27.	Contour plot of omnidirectional bi-variate return period values for 1, 10, 50 and 100 year ARIs for significant wave height and peak wave period at Sites WB1 (top) and A1 (bottom). The dark crosses correspond to the estimated deterministic $H_s$ and associated $T_p$ return period values for each ARI (years) indicated in this legend. ....	39
Figure A.1	Measured and hindcast wind rose at 10 m extracted at Hicks Bay between 2000 and 2008. ....	42

## LIST OF TABLES

Table 2.1	Extents, resolution and frequency range defined for the four SWAN nests. Each child domain was run off spectral wave boundaries provided by the domain immediate above in the table. Spectral boundaries to run the NZN parent nest were prescribed from the 0.5° global WW3 wave model. ....	12
Table 2.2	Geographic coordinates, observational durations, samplings, record levels and water depths corresponding to the ADCP and S4 current meter deployments over Poverty Bay and the adjacent shelf margin. ....	15
Table 3.1	Comparison between measured and hindcast wind data. Accuracy measures for wind speed at Gisborne Airport between 2000 and 2008. ....	20
Table 3.2	Comparison between measured and hindcast wave data. Accuracy measures for significant wave height ( $H_s$ ) and peak wave period ( $T_p$ ) at sites BND, WB1 and A1.....	23
Table 3.3	Comparison between measured and (bias-corrected) hindcast wave data. Accuracy measures for significant wave height ( $H_s$ ) at sites WB1 and A1.....	30
Table 3.4	Total and monthly significant wave height statistics at Site WB1 based on 10 year hindcast (1996 – 2005). ....	36
Table 3.5	Total and monthly significant wave height statistics at Site A1 based on 10 year hindcast (1996 – 2005). ....	36
Table 3.6	Omnidirectional $H_s$ and associated $T_p$ return period values for 1, 10, 50 and 100 year ARIs using the 10 year hindcast data at Sites WB1 and A1.....	39

## 1. INTRODUCTION

Eastland Port Ltd are seeking to renew their maintenance dredging and disposal consents at the Port of Gisborne.

Currently, dredged sediment is disposed at an offshore disposal site situated in approximately 18 – 20 m water depth (**Error! Reference source not found.**), with an average annual rate of approximately 73,000 m<sup>3</sup> based on estimates obtained between 2002 and 2019 by Eastland Port.

Maintenance dredging is expected to occur using the Trailing Suction Hopper Dredge (TSHD) “Pukunui” although, if there are significant inflows of sediment due to large storm events, a higher productivity Trailing Suction Hopper Dredge (TSHD) may be required to ensure the required port and channel depths can be maintained. It is likely that some maintenance dredging may also be undertaken using a Backhoe Dredger (BHD) or Cutter Suction Dredger (CSD).

MetOcean Solutions (MOS) has been contracted to provide coastal oceanographic expertise to investigate both physical and morphological effects and associated sediment transport patterns resulting from the dredging and disposal of maintenance dredging material at the current disposal site.

For this purpose the numerical wave transformation model Spectral Wave Nearshore (SWAN) has been used to characterise the wave climate, both within and offshore Poverty Bay (see flow chart in Figure 1.2). A multiple-nesting approach was applied to produce a 10-year wave hindcast for Poverty Bay. Measured wave data has been used to calibrate and validate the numerical model.

The applied methodology is provided in Section 2. It includes a description of the model setup, forcing and boundary conditions, validation methods and available measured datasets. Results of the validation process and wave climate analysis are provided and discussed in Section 3. A brief summary is presented in Section 4 while the references are cited in Section 5.

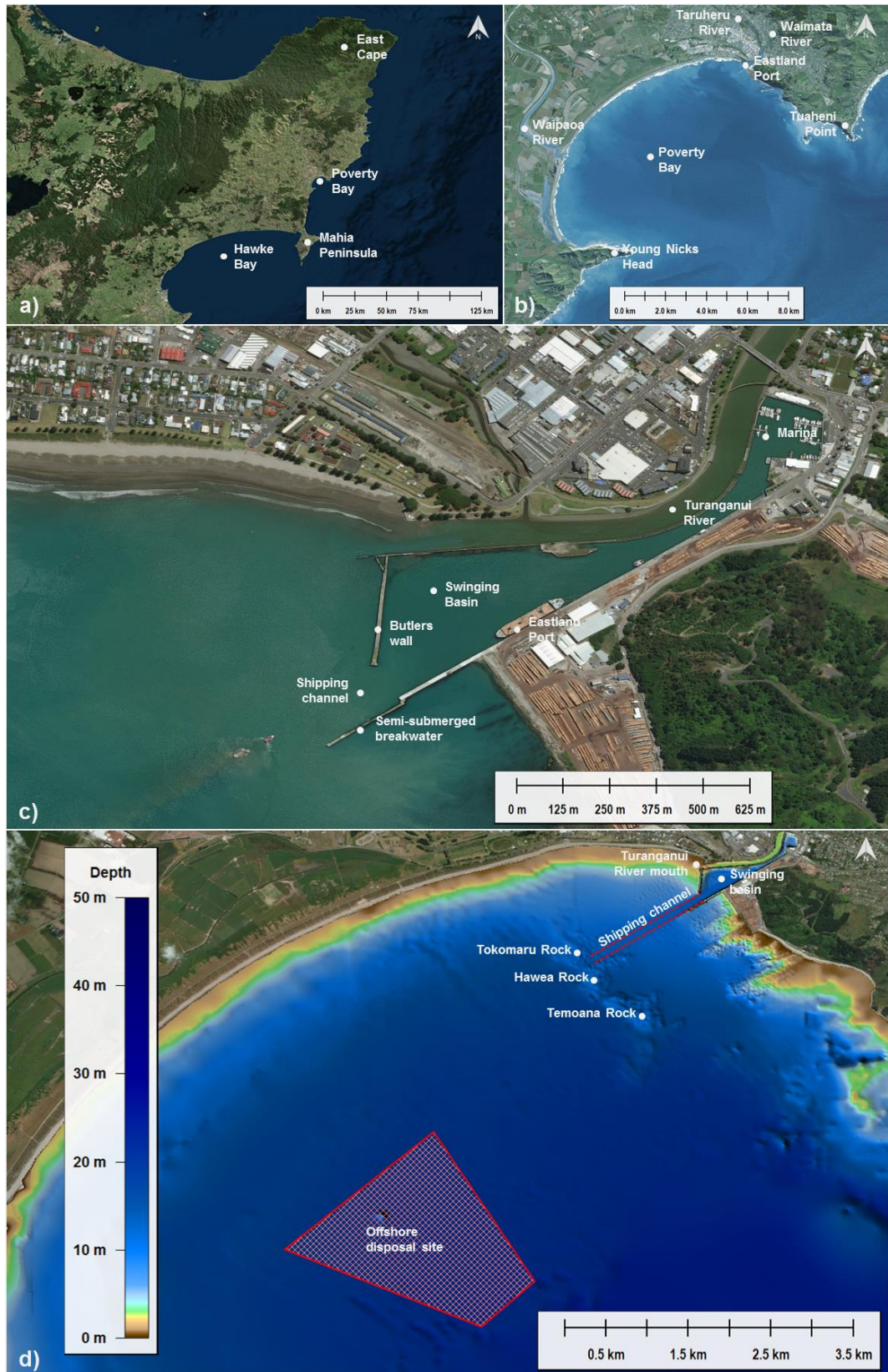


Figure 1.1 Maps showing the location of Poverty Bay (a and b), and Eastland Port (c) with the locations used in the present study. Both offshore disposal and shipping channel are indicated on top of the bathymetry in (d).

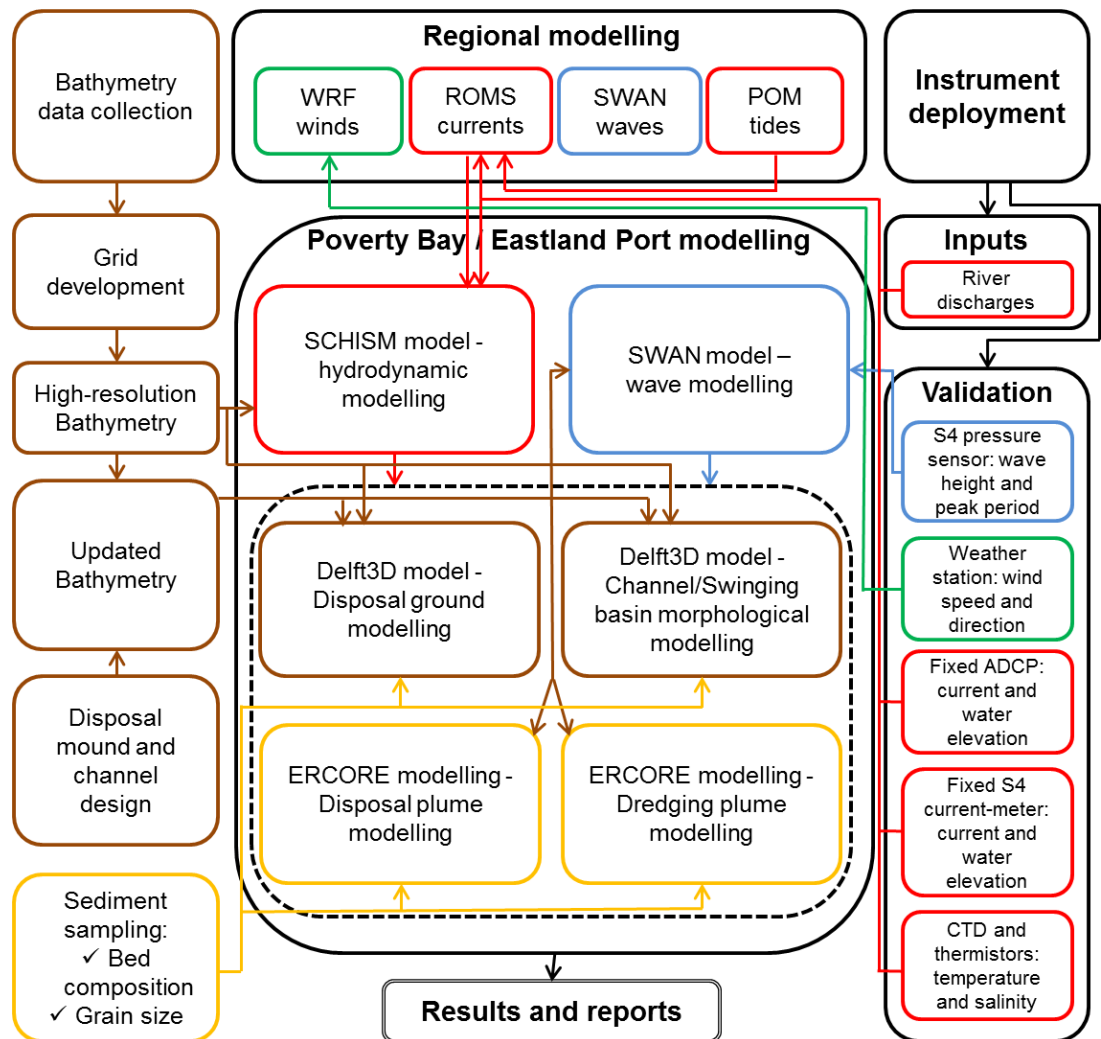


Figure 1.2 Flow chart showing the numerical modelling process for the study. Red lines indicate hydrodynamics; blue indicates waves; green indicates wind and brown indicate bathymetry and yellow lines indicate sediments.

## 2. MODEL METHODS

### 2.1. Bathymetry

Bathymetry is an essential requirement for coastal numerical modelling. MetOcean Solutions has compiled an extensive national and regional bathymetric dataset derived from Electronic Navigation Charts (ENC). These datasets were updated with hydrographic surveys carried out within Eastland Port and the surroundings. Specialist data manipulation tools have been used to allow the merging, interpolation and QA of raw bathymetry data when establishing numerical model domains. Note that GEBCO data (Becker et al., 2009) was also used to characterise the deepest offshore areas.

Water depth in the regional wave models was derived from a 500 m gridded bathymetry shown in Figure 2.1 (top). A 5 x 5 m gridded bathymetry (Figure 2.1, bottom) was used to interpolate to the computational grid in SWAN.

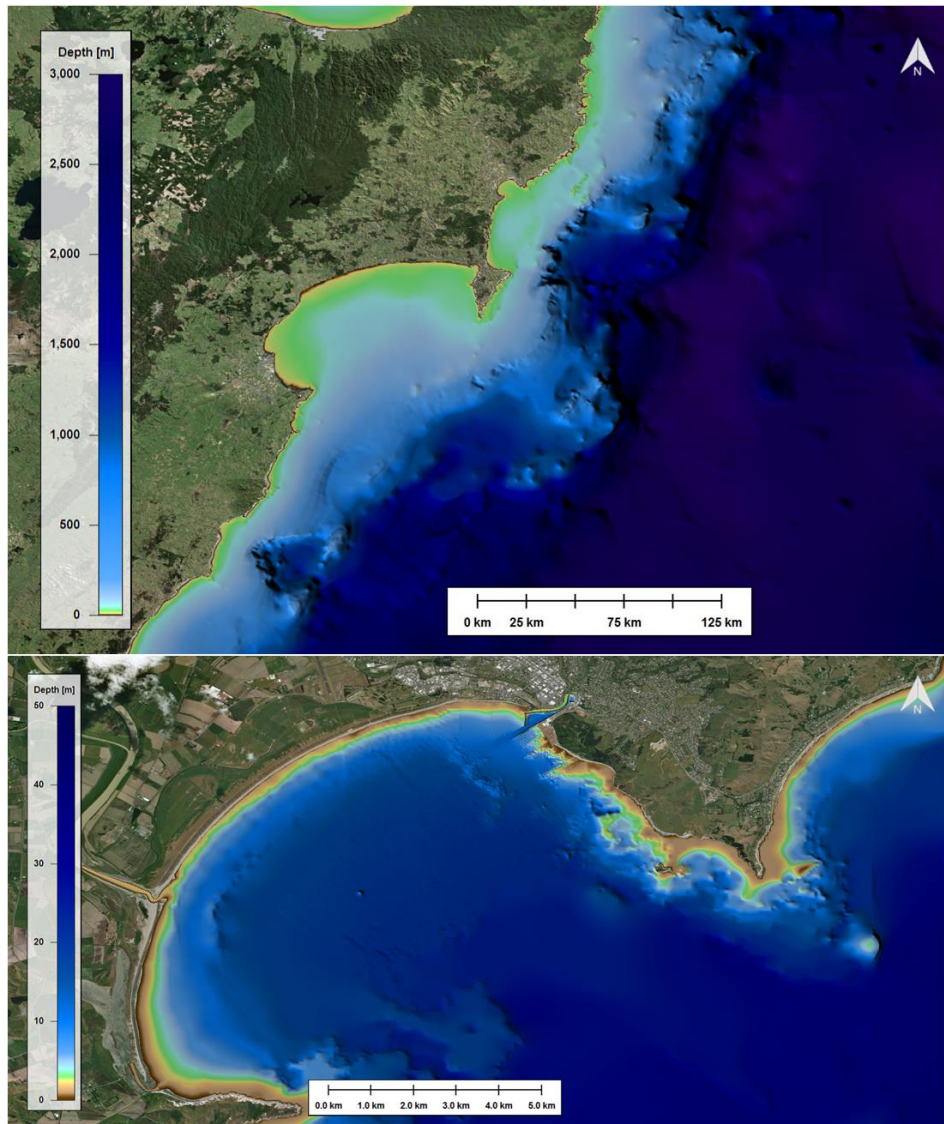


Figure 2.1 Map showing both the 500 x 500 m (top) and the 5 x 5 m (bottom) gridded bathymetries used to interpolate the water depth to the computational grid in SWAN.

## 2.2. Model description

Wave modelling was undertaken using a modified version of SWAN<sup>1</sup>, calibrated over years 2007 and 2008 and used to run a high-resolution, 10-year hindcast of the Poverty Bay region spanning 1996 to 2005.

SWAN is a third generation ocean wave propagation model which solves the spectral action density balance equation. The model simulates the growth, refraction and decay of each frequency-direction component of the complete sea state, providing a realistic description of the wave field as it changes in time and space. Physical processes that are modelled include the generation of waves by surface wind, dissipation by white-capping, resonant nonlinear interaction between the wave components, bottom friction and depth limited wave breaking energy dissipation.

A detailed description of the model equations, parameterisations and numerical schemes can be found in Holthuijsen et al., (2007) or the SWAN documentation<sup>2</sup>.

## 2.3. Model Setup

SWAN was run in the non-stationary mode with all third generation physics included in the model. The source term parameterisations of Van der Westhuysen et al. (2007) were employed and the Collins, (1972) scheme was used for bottom friction. The spectra were discretised with 36 directional bins (10° directional resolution) and logarithmic frequencies starting at 0.0412 Hz and extending up to 1.4003 Hz for the highest resolution nests (see Table 2.1), with resolution  $\Delta f = 0.1f$ .

A downscale nesting approach was employed to resolve the nearshore region around Eastland Port (Figure 2.2). Four regular nests were defined with resolutions progressively increasing from of 4 km and 20 m (Table 2.1).

A regional atmospheric hindcast using the Weather and Research Forecasting (WRF) was used to provide atmospheric forcings to SWAN. The WRF dataset was run over New Zealand at approximately 12 km resolution. Boundary conditions were derived from the global Climate Forecast System Reanalysis (CFSR)<sup>3</sup>. This leap of resolution from the 35 km available from CFSR (23 km after 2011) adds accuracy and variability to the atmospheric fields that force the wave model.

Full spectral boundaries for the coarser SWAN domain were prescribed from a global implementation of WAVEWATCH III (WW3) spectral wave model (Tolman, H.L., (1991) run at 0.5° resolution using the source term parameterisations of Ardhuin et al., (2010).

---

<sup>1</sup> Modified from SWAN version of the 40.91 release

<sup>2</sup> [http://swanmodel.sourceforge.net/online\\_doc/online\\_doc.htm](http://swanmodel.sourceforge.net/online_doc/online_doc.htm)

<sup>3</sup> <https://climatedataguide.ucar.edu/climate-data/climate-forecast-system-reanalysis-cfsr>

Table 2.1 Extents, resolution and frequency range defined for the four SWAN nests. Each child domain was run off spectral wave boundaries provided by the domain immediate above in the table. Spectral boundaries to run the NZN parent nest were prescribed from the 0.5° global WW3 wave model.

Domain	Longitude (degree)			Latitude (degree)			Frequencies (Hz)	
	West	East	Res	South	North	Res	Lowest	Highest
NZN	170.00	180.00	0.0400	-43.000	-34.0000	0.0400	0.0412	0.7186
Gisborne	177.75	178.50	0.0050	-39.330	-38.5800	0.0050	0.0412	1.0521
Poverty Bay	177.93	178.11	0.0008	-38.780	-38.6696	0.0008	0.0412	1.4003
Eastland	178.00	178.05	0.0002	-38.704	-38.6696	0.0008	0.0412	1.4003

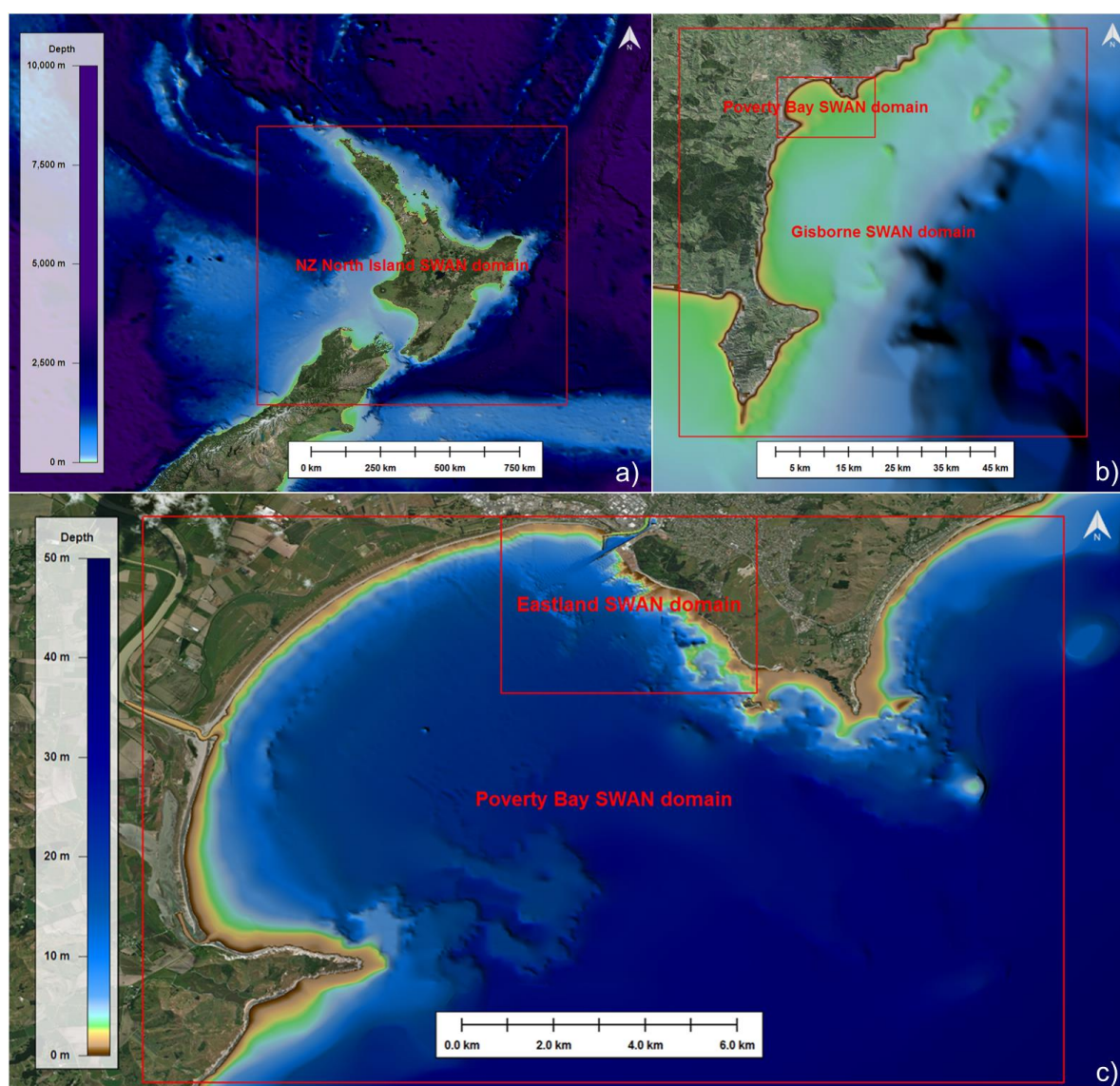


Figure 2.2 Map showing the SWAN nested domains used to simulate the spectral transformation of the offshore wave climates to the nearshore zone. Information specific to each set-up is provided in Table 2.1.

## 2.4. Post-processing

In order to validate the SWAN model, two-dimensional wave spectra  $E(f, \theta)$  were output at hourly intervals at sites where wave measurements were available.

Spectral moments were calculated as:

$$m_x = \iint f^x E(f, \theta) df d\theta, \quad (\text{Eq. 2.1})$$

where  $f$  and  $\theta$  are the wave frequency and direction, and  $x$  is an integer. The significant wave height  $H_s$ , the mean direction at the peak wave frequency  $D_{pm}$  and the peak wave period  $T_p$  were defined as:

$$H_s = 4\sqrt{m_0}, \quad (\text{Eq. 2.2})$$

$$D_{pm} = \tan^{-1} \frac{\int_{-\pi}^{\pi} E(f_p, \theta) \sin \theta d\theta}{\int_{-\pi}^{\pi} E(f_p, \theta) \cos \theta d\theta} \quad (\text{Eq. 2.3})$$

$$T_p = 1/f_p, \quad (\text{Eq. 2.4})$$

where  $f_p$  is the peak wave frequency of the one-dimensional spectrum:

$$E(f) = \int_{-\pi}^{\pi} E(f, \theta) d\theta. \quad (\text{Eq. 2.5})$$

## 2.5. Model uncertainty and validation methods

The wave model performance is dependent on a number of factors. While some of them are intrinsic to the model itself (physics, discretisation, etc.), a considerable degree of uncertainty comes from the inputs. Comparisons between model data and observations at several sites were carried out in the present study to demonstrate the ability of the model to replicate adequately both the offshore and nearshore wave climate. This process is particularly important for decision makers as it places the model results into context and helps for a better interpretation of the model outputs.

### 2.5.1. Wind validation

The 12 km WRF hindcast used to force the SWAN domains was validated against measured surface wind data from the Gisborne Airport. Gisborne Airport is surrounded by mountains and partially sheltered from north-easterly winds due to the topographical characteristic of the embayment. For this reason, the Hicks Bay site was also used as a control site during the validation process. Using both sites highlighted the potential effect of the topographical relief on the model accuracy at Gisborne. The wind validation is presented in Section 3. Additional results are provided in Appendix A.

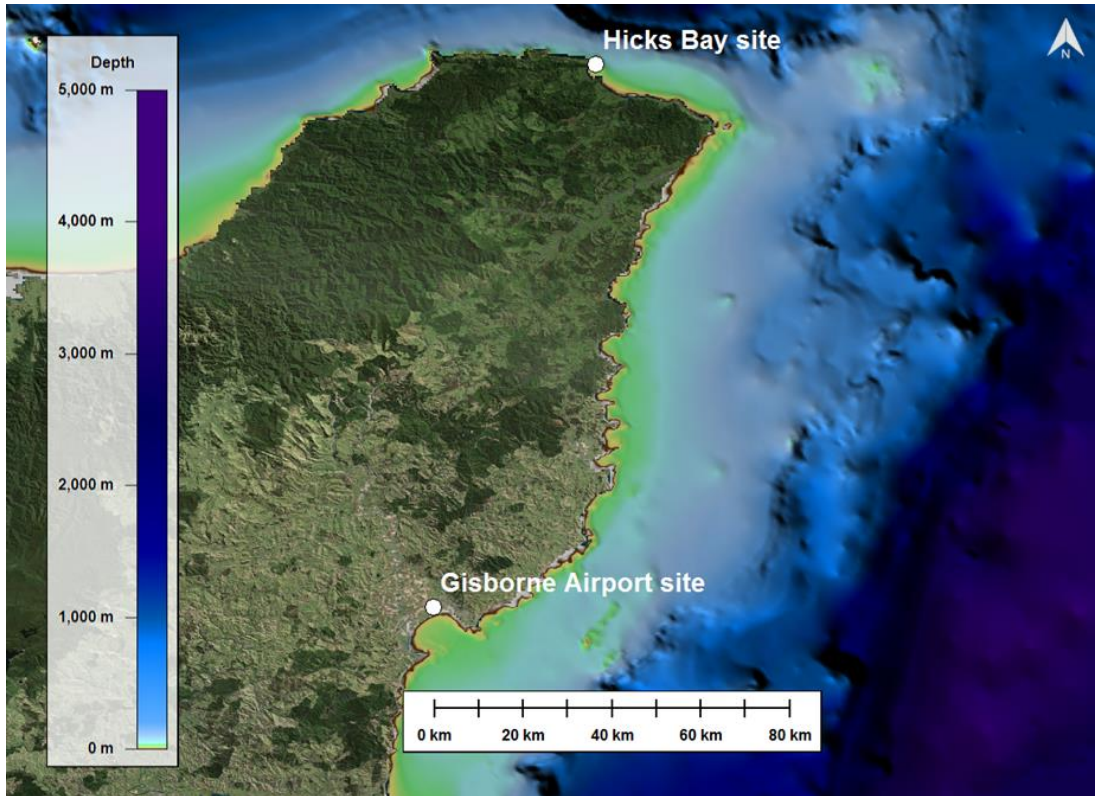


Figure 2.3 Map showing the regional bathymetry of the continental shelf between Gisborne and East Cape. The white dots indicate the sites used to compare hindcast and measured wind data collected by weather stations.

### 2.5.2. Wave validation

Model validation and bias correction was undertaken using the measured data between 2007 and 2008 from the wave buoy within Poverty Bay (site WB1, Table 2.2 and Figure 2.4). Significant wave height, maximum wave height, peak wave period and direction, mean wave period and direction, directional spreading, and other relevant wave parameters were averaged over 20 and 40-min periods.

In addition, the predicted significant wave heights from the model were compared to the measured wave data from an S4 current meter with a pressure sensor at site A1 near Eastland Port (Table 2.2 and Figure 2.4). This provided an evaluation of the model capacity to replicate the near shore wave climate and the wave climate near the port. Site A1 is located just north of the shipping channel in approximately 8-metres water depth, and partially sheltered by the complex shallow reef offshore Kaiti Beach.

A description of the instrument deployments including geographic coordinates, observational durations, samplings, record levels and water depths are summarised in Table 2.2. Results of the model skill assessment, including accuracy measurements and plots, are provided in Section 3.

Table 2.2 Geographic coordinates, observational durations, samplings, record levels and water depths corresponding to the ADCP and S4 current meter deployments over Poverty Bay and the adjacent shelf margin.

Site	Instrument	Coordinates (WGS84)		Observational durations		Sampling	Water depth (m)
		Longitude (E)	Latitude (N)	Start date	End date		
A1	S4 current meter + pressure sensor	178.0173	-38.677	27/08/2014	19/11/2014	½ sec during 20 min every 60 min	8
WB1	Wave buoy	178.0107	-38.698	01/07/2007	31/01/2008	20 min to 40 min averages	20

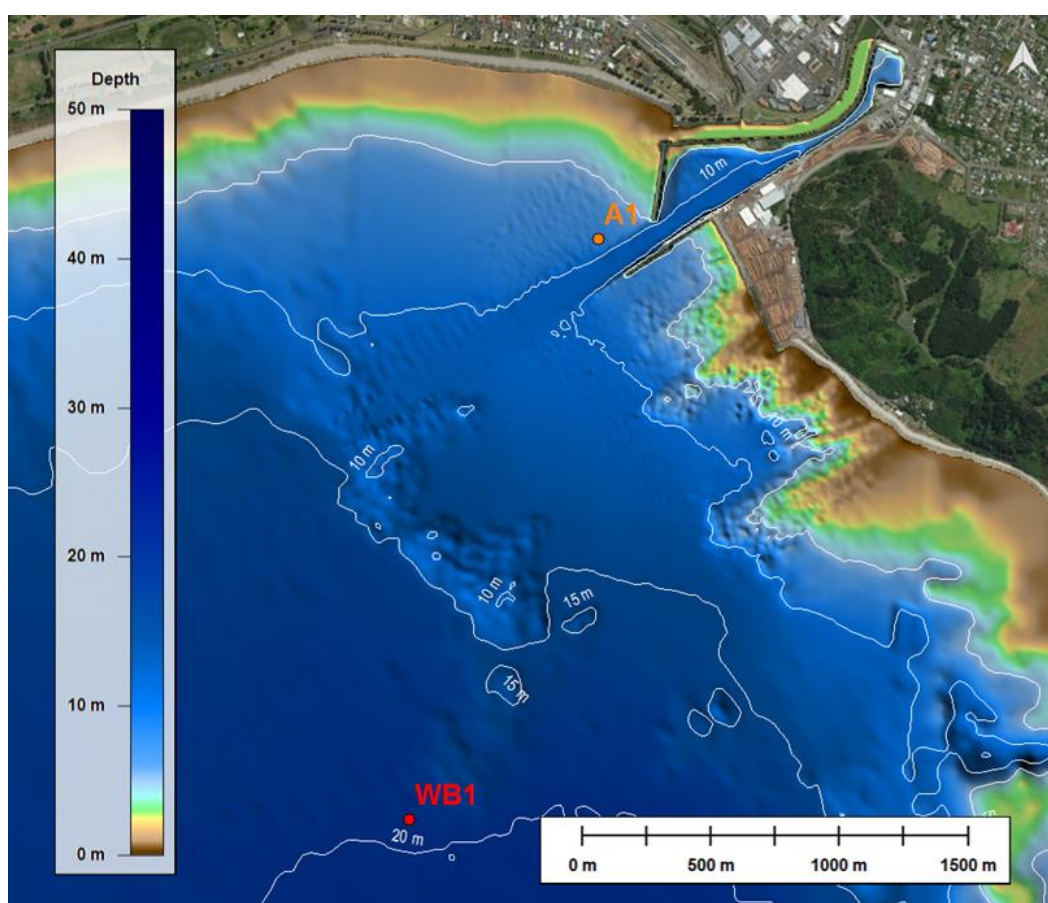


Figure 2.4 Map showing the bathymetry over Poverty Bay. The orange dots indicate the location of the S4 current meter data used to validate the SWAN wave model.

### 2.5.3. Evaluation criteria

The predictive skill assessment of the SWAN numerical model was undertaken based on the quantitative agreement between model and measured wave characteristics at several sites within the study area. The following quantitative accuracy parameters were calculated:

Mean Absolute Error (MAE):

$$MAE = \frac{1}{N} \sum_{i=1}^N |M_i - O_i| \quad (\text{Eq. 2.6})$$

Root Mean Square Error (RMSE):

$$RMSE = \sqrt{\frac{1}{N} \sum_{i=1}^N (M_i - O_i)^2} \quad (\text{Eq. 2.7})$$

Mean Relative Absolute Error (MRAE):

$$MRAE = \frac{1}{N} \sum_{i=1}^N \frac{|M_i - O_i|}{O_i} \quad (\text{Eq. 2.8})$$

Bias:

$$Bias = \frac{1}{N} \sum_{i=1}^N (M_i - O_i) \quad (\text{Eq. 2.9})$$

Scatter Index (SI):

$$SI = \frac{\sqrt{\frac{1}{n} \sum_{i=1}^N ((M_i - \bar{M}) - (O_i - \bar{O}))^2}}{\bar{O}} \quad (\text{Eq. 2.10})$$

where  $M_i$  and  $O_i$  are the modelled and observed  $H_s$ ,  $N$  is the number of collocations and the overbar denotes the mean value.

The wave model was validated for both significant wave height  $H_s$  and peak wave period  $T_p$ . At location A1, waves were measured from a pressure sensor near the seabed and higher frequencies (period < 5 s) were excluded when deriving the spectra (due to frequency attenuation with depth). To insure consistence, the same frequency cut-off was applied to the model spectra when calculating the spectral wave parameters at A1.

### 2.5.4. Bias correction technique

Global wave models can exhibit systematic errors in some areas that propagate through the dynamic downscaling from offshore to nearshore areas. To improve model skills, a bias-correction technique was applied to the wave hindcast based on the  $H_s$  percentiles between model and measured wave data at site WB1. The technique involved calculating a 1-degree polynomial using co-located data from

years 2007–2008 and applying the coefficients to correct modelled  $H_s$  within the Poverty Bay and Eastland SWAN domains. The polynomial was defined by:

$$H_{s,corr}(x, y, t) = 1.23H_s(x, y, t) - 0.11. \quad (\text{Eq. 2.11})$$

The relation was assumed valid throughout the Poverty Bay area. Results of the bias correction are presented in Section 3.3.

## **3. RESULTS**

This section provides an assessment of the model performance as well as an overview of the wave climate within Poverty Bay and near Eastland Port. A quantitative validation of both wind and wave climates are presented in Section 3.1. Comparison between measured and bias-corrected hindcast data are also included to show the degree of improvements provided by the bias-correction technique described in Section 2.5.4. Section 3.2 provides wave statistics at sites A1 and WB1 based on the bias-corrected hindcast data.

### **3.1. Quantitative validation**

#### **3.1.1. Wind validation**

The modelled hindcast wind velocities at 10 m (as used to force both SWAN wave and ROMS and SCHISM hydrodynamic models) were compared against observations from the Gisborne Airport weather station. The time series of model and measured wind speed for the period June 2002 - June 2003 are shown in Figure 3.1.

The quantitative validation (Figure 3.2) showed the model to exhibit a reasonable correspondence with the measured data. On average, hindcast wind speeds were biased slightly high by  $\sim 0.75 \text{ m.s}^{-1}$ , while peak wind speeds were biased slightly low (by  $1\text{-}2 \text{ m.s}^{-1}$ ,

Table 3.1).

Comparisons of the model and measured wind roses are provided in Figure 3.3, and show a good directional correlation, with predominant NW octant winds in both model and measured data, consistent with the findings of Chappell, (2016).

In general, measured winds at Gisborne Airport tend to be primarily orientated NW/SE. In comparison, modelled winds tend to display more directional variance; due to the topographical sheltering effect afforded by Poverty Bay not being fully captured in the 12 km resolution atmospheric model.

To evaluate if this directional bias was mainly constrained to the Poverty Bay embayment a comparison between the measured and model wind data at Hicks Bay, located at East Cape (Figure 2.3), was undertaken. This area is one of the most exposed locations along the East Coast where measured wind data are available. Measured and model wind roses from Hicks Bay are provided in Appendix A, and show the model data to accurately capture the climatic variability in the wind fields at this more exposed site, suggesting the disparity between modelled and measured wind climates at the Gisborne Airport is due to topographical effects not fully represented within the model.

The effect of not fully capturing the SE events within the wave hindcast in Poverty Bay on the wave and current outcomes (SWAN and ROMS/SCHISM) is not expected to be significantly in terms of quantifying the wave and current climatic variability.

Table 3.1 Comparison between measured and hindcast wind data. Accuracy measures for wind speed at Gisborne Airport between 2000 and 2008.

Statistics	Wind speed (m.s <sup>-1</sup> )
MAE	2.24
RMSE	2.85
MRAE	0.93
Bias	0.75
Scatter Index	0.6

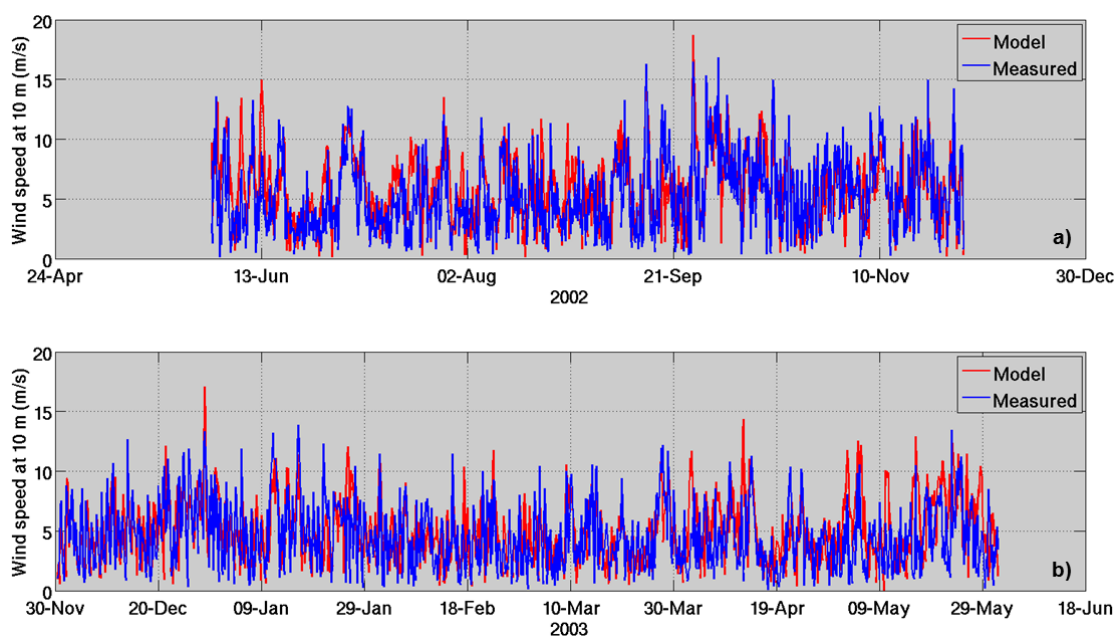


Figure 3.1 Measured and modelled wind speed at 10 m between June and December 2002 (a), January and June 2003 (b).

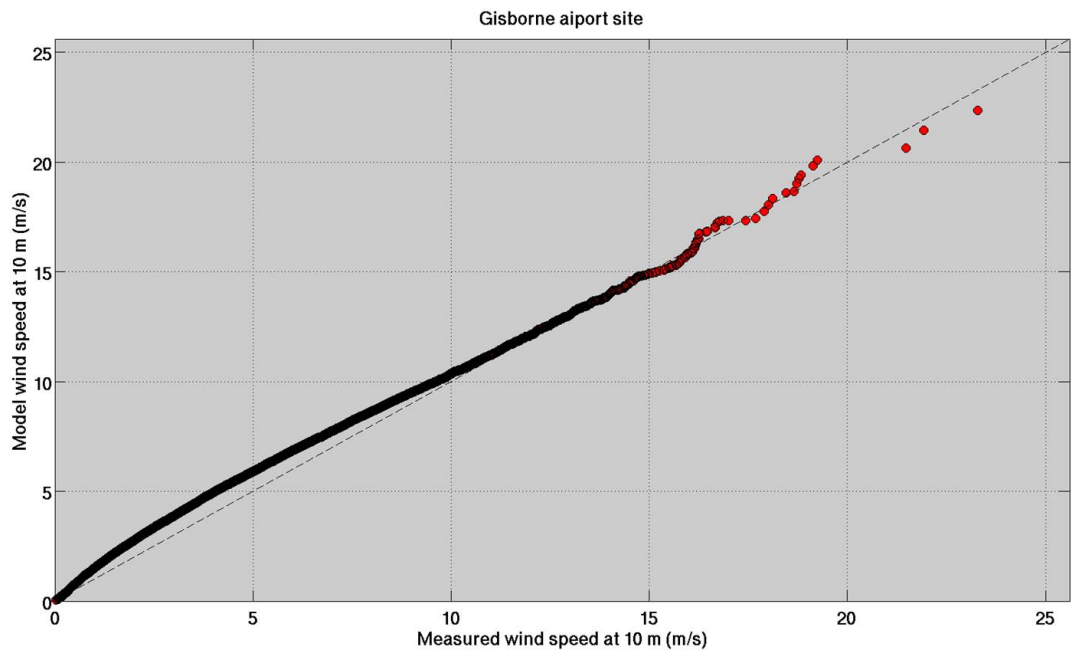


Figure 3.2 Quantile-Quantile plot of the 10 m measured and model wind speeds at Gisborne Airport for the period 2000 – 2008.

### Gisborne Airport [177.9860 E; 38.6610 S]

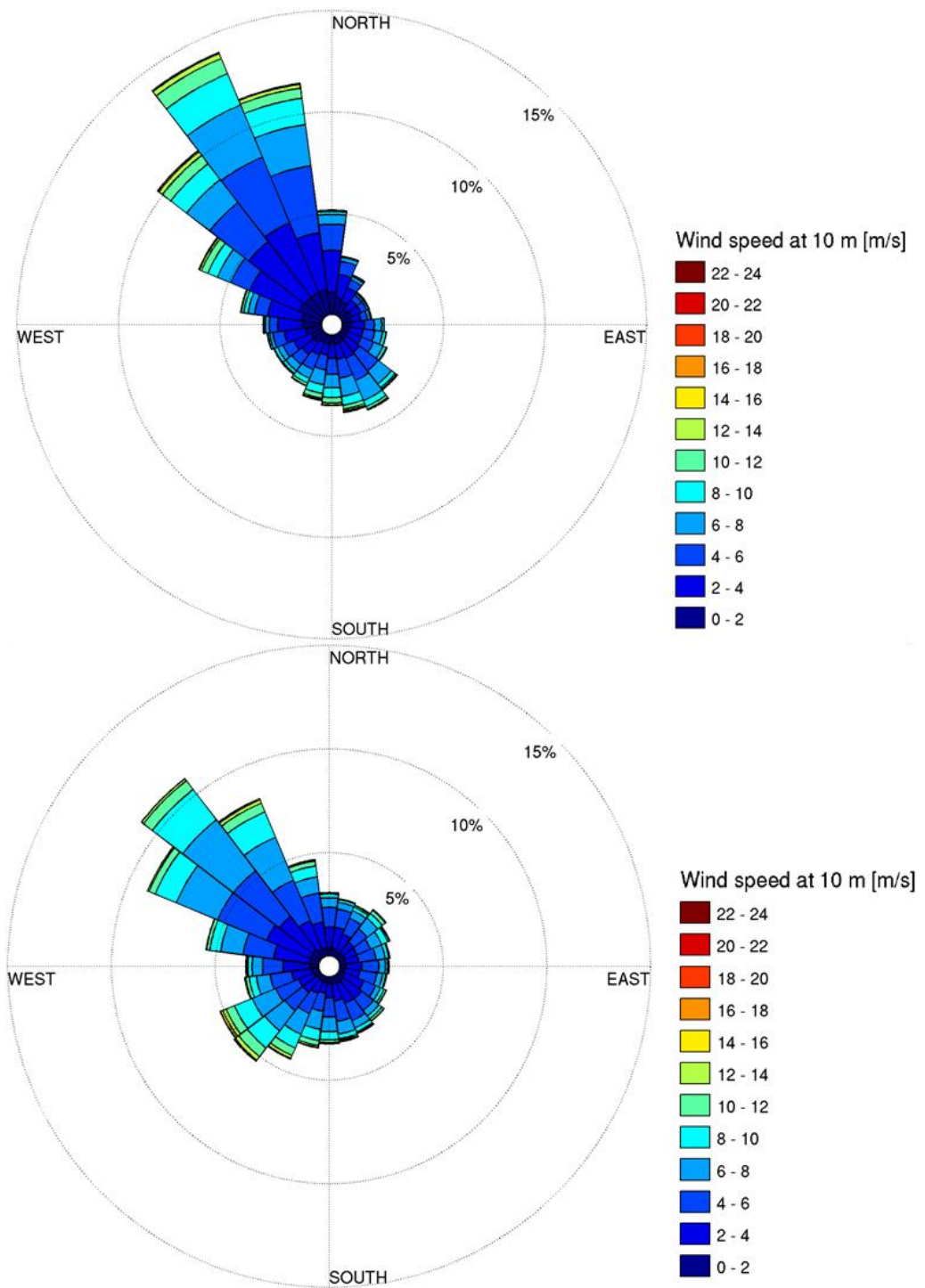


Figure 3.3 Measured (top) and model (bottom) wind roses at Gisborne Airport for the period 2000 – 2008. Winds are reported in the “coming from” directional reference.

### 3.1.2. Wave validation

Comparison between measured and modelled significant wave height at Site WB1 show that the SWAN wave model tended to under-predicts large wave events. Analysis undertaken in 2012 (Figure 3.4) suggested that this low bias is largely driven by missing swell wave energy generated during extra-tropical cyclone events to the East–Southeast of Poverty Bay (e.g., Figure 3.5). These events typically developed outside the boundaries of the SWAN domains and were not perfectly represented in the global models. This hypothesis was investigated by comparing  $H_s$  from the global wave model against data from satellite altimeters over a region near the eastern boundary of the NZN SWAN domain, limited by 180 – 183 E, 43 – 37 S (Figure 3.6). Model and satellite  $H_s$  were collocated within 0.5° by 0.5° bins within this area. Results from the offshore validation are shown in Figure 3.7 and Figure 3.8. An overall negative bias of 14 cm was observed which was mainly driven by under-predicting high-energy events.

Significant wave height was well represented in the model at the nearshore site A1. A positive bias of only 9 cm was observed in the model (Table 3.2) and most of the main events were relatively well captured (Figure 3.12).

The modelled peak wave period  $T_p$  closely matched observed values at the two locations. Error measures were relatively small at both sites, with  $T_p$  under 1 s and RMSE around 2.5 s (Table 3.2). Frequent bimodal conditions in the region means some scatter in  $T_p$  occurs where the relative contribution between wind- and swell-dominated conditions changes between model and data (see Figure 3.13 to Figure 3.16). However the majority of the data agree well at both sites.

Table 3.2 Comparison between measured and hindcast wave data. Accuracy measures for significant wave height ( $H_s$ ) and peak wave period ( $T_p$ ) at sites BND, WB1 and A1.

Sites	Parameters	Bias	RMSE	MAE	MRAE	Scatter Index
BND	$H_s$ [m]	-0.14	0.38	0.28	0.11	0.13
WB1	$H_s$ [m]	-0.10	0.26	0.18	0.18	0.24
	$T_p$ [s]	-0.6	2.6	1.6	0.16	0.22
A1	$H_s$ [m]	0.09	0.18	0.14	0.36	0.34
	$T_p$ [s]	-0.6	2.4	1.7	0.14	0.19

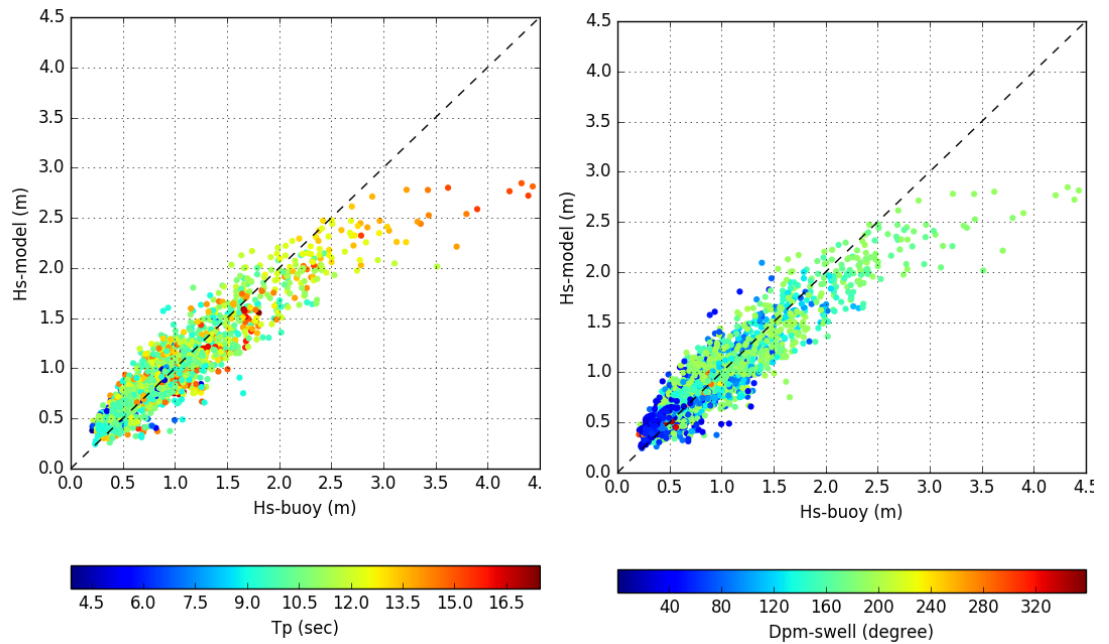


Figure 3.4. Model versus measured significant wave height  $H_s$  at the WB1 location during the year of 2012. Colours represent modelled (left) peak wave period  $T_p$  and (right) mean wave direction at the peak wave frequency ( $D_{pm}$ ) at an offshore reference site located at 178.3 E, 39.0 S.

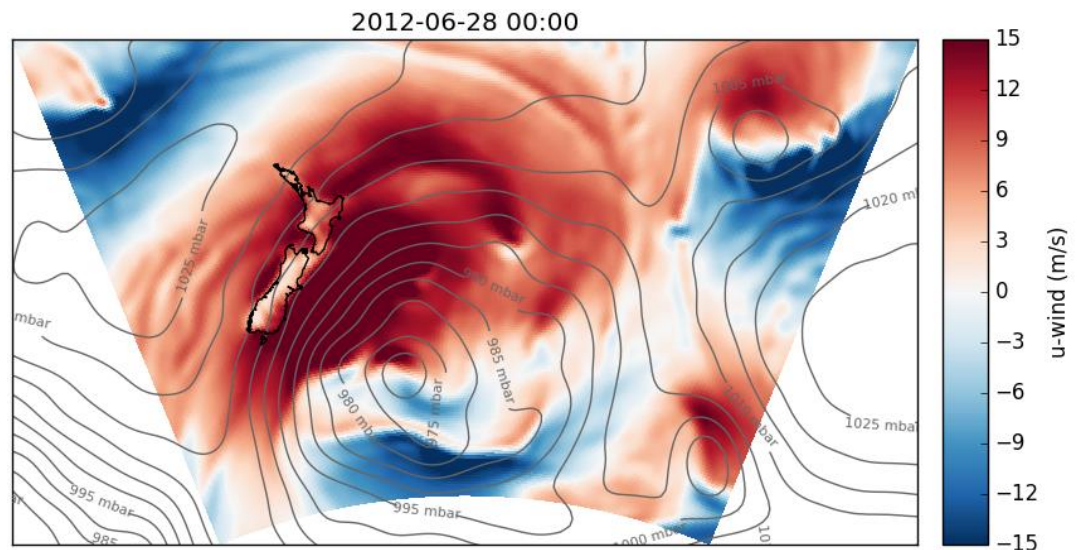


Figure 3.5. Snapshot of wind velocities and mean sea level pressure during a low-pressure system on 28 June 2012.

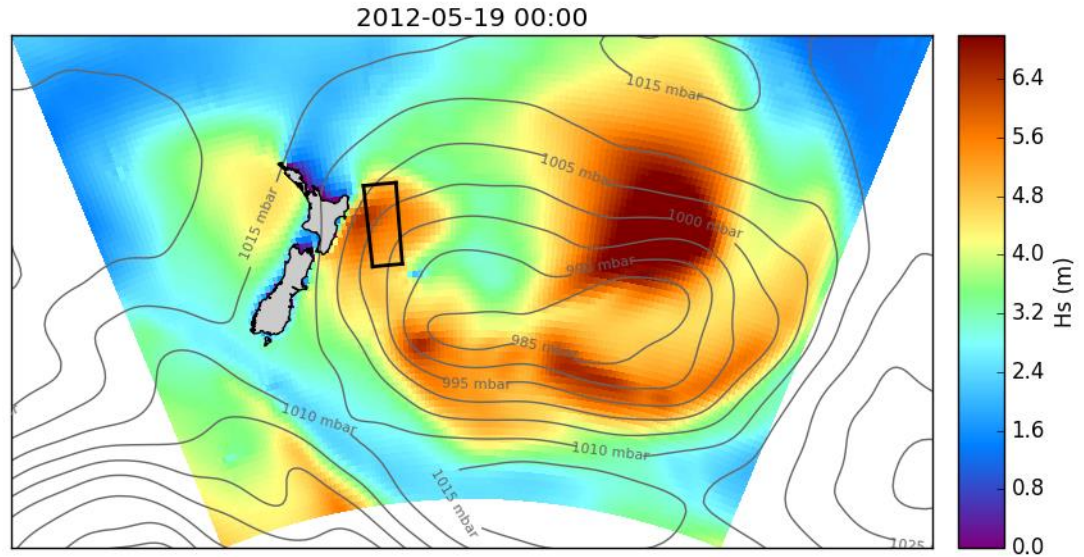


Figure 3.6. Snapshot of significant wave height  $H_s$  during a low-pressure system on 19 May 2012. The rectangle limited by 180 – 183 E, 43 – 37 S shows the area over which  $H_s$  from the global wave model and satellite altimeters were collocated.

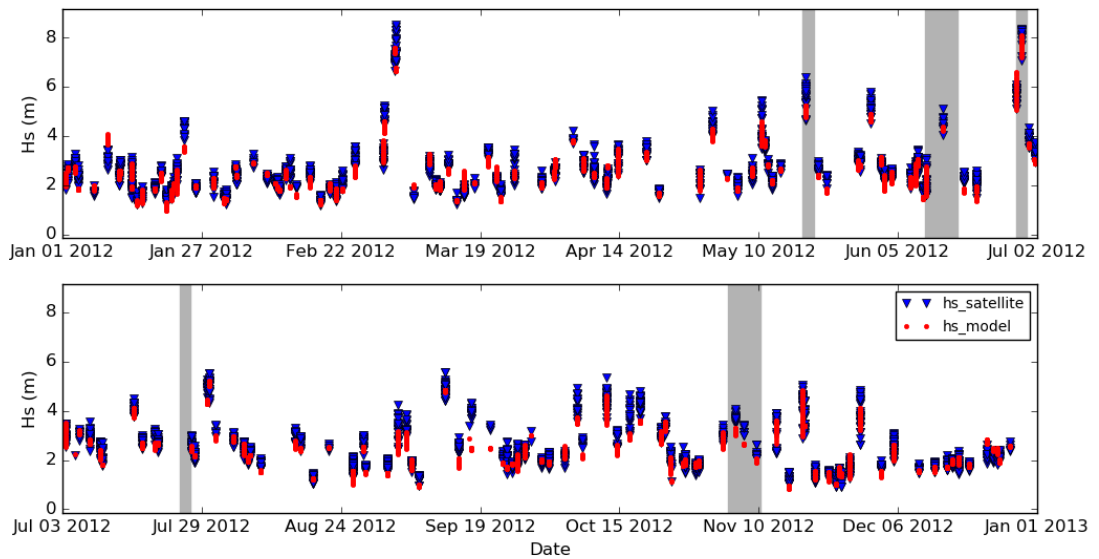


Figure 3.7. Time series of satellite altimeter and modelled significant wave height  $H_s$  collocated within  $0.5^\circ$  by  $0.5^\circ$  bins over the area delimited by 180 – 183 E, 43 – 37 S (see Figure 3.6) during 2012. Gray patches show identified periods influenced by extra-tropical cyclones (e.g. Figure 3.5) when waves were observed to be strongly under predicted at location WB1 (corresponding to the high-energy, long-period SE events shown in Figure 3.4). Note data from WB1 were scarce before May 2012 and the high-energy events earlier in the year shown here are not represented in Figure 3.4.

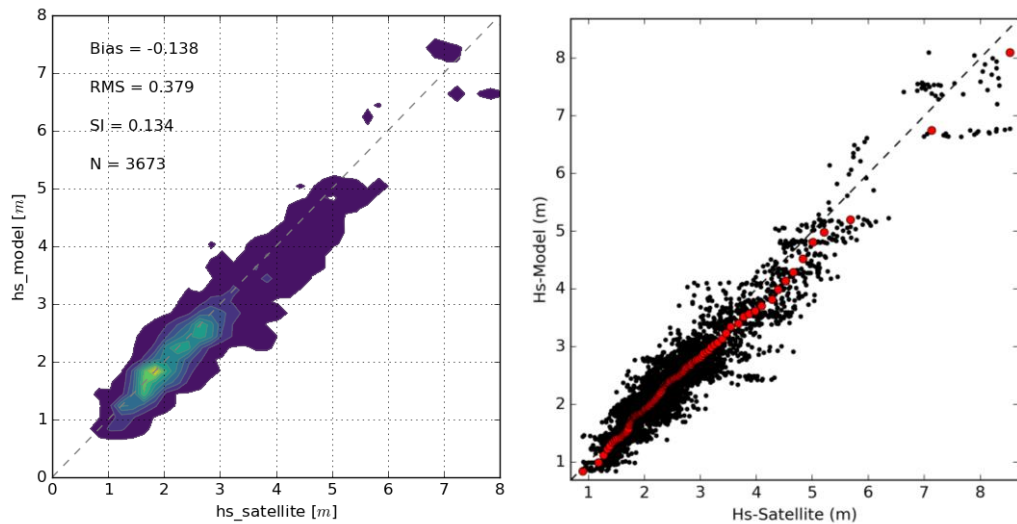


Figure 3.8. Scatter density (left) and scatter diagram (right) comparing satellite altimeter and modelled significant wave height  $H_s$  over the area limited by 180 –183 E, 43 – 37 S (see Figure 3.6) during 2012. Hot colours on the left indicate higher density of data-points. Red circles on the right show the quantile-quantile at the 0.01 percentile.

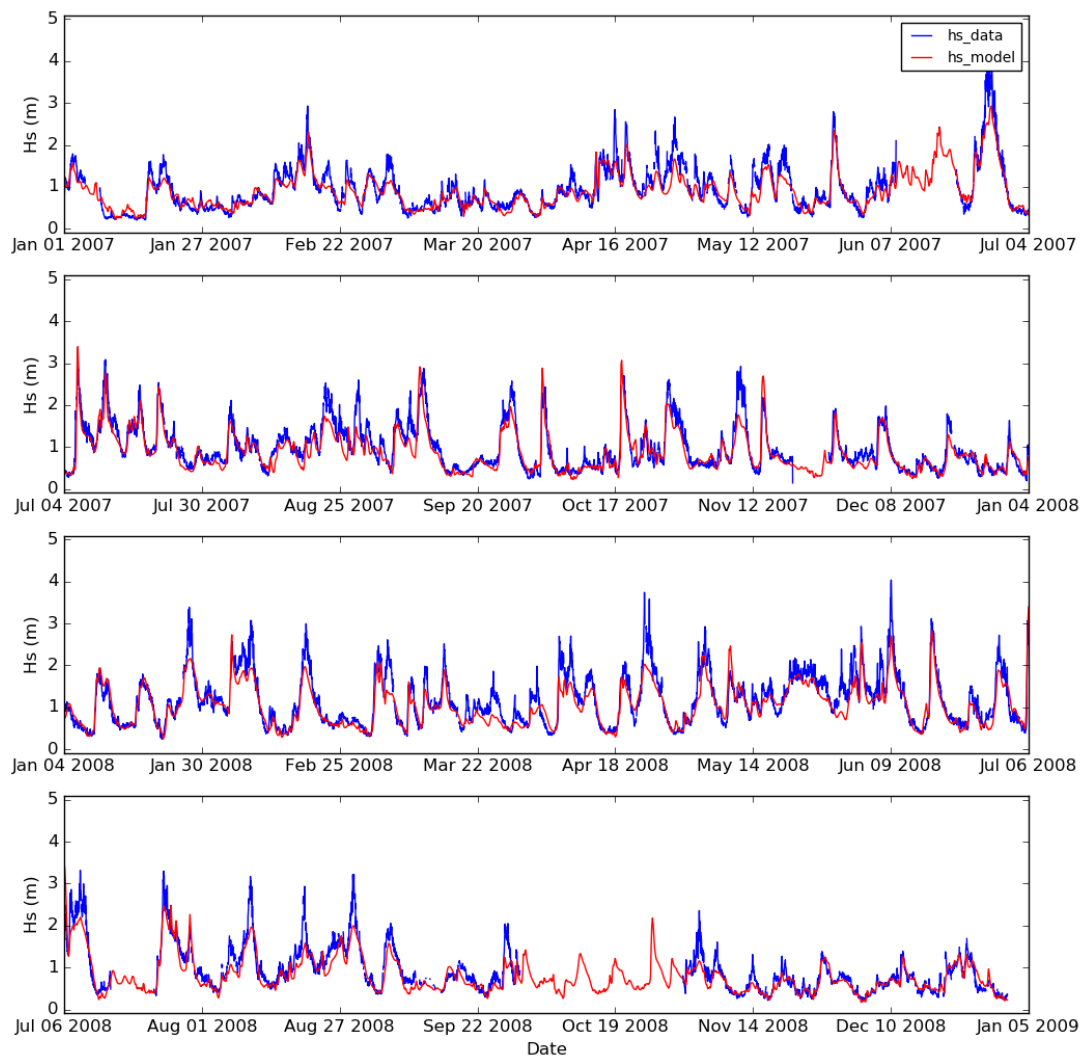


Figure 3.9. Time series of measured and modelled significant wave height  $H_s$  at site WB1 between 2007 – 2008.

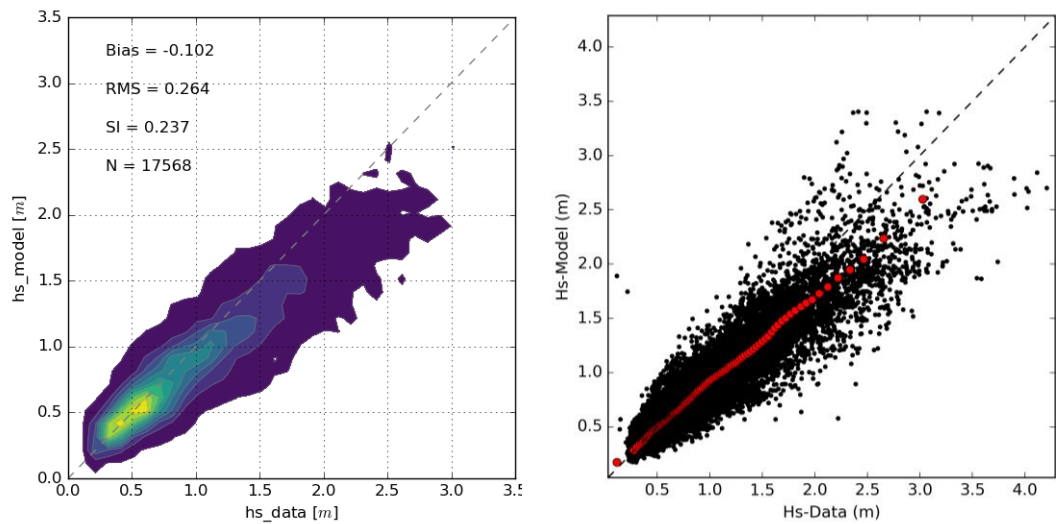


Figure 3.10. Scatter density (left) and scatter diagram (right) comparing measured and modelled significant wave height  $H_s$  at WB1 site for years 2007–2008. Hot colours on the left indicate higher density of data-points. Red circles on the right show the quantile-quantile at the 0.01 percentile.

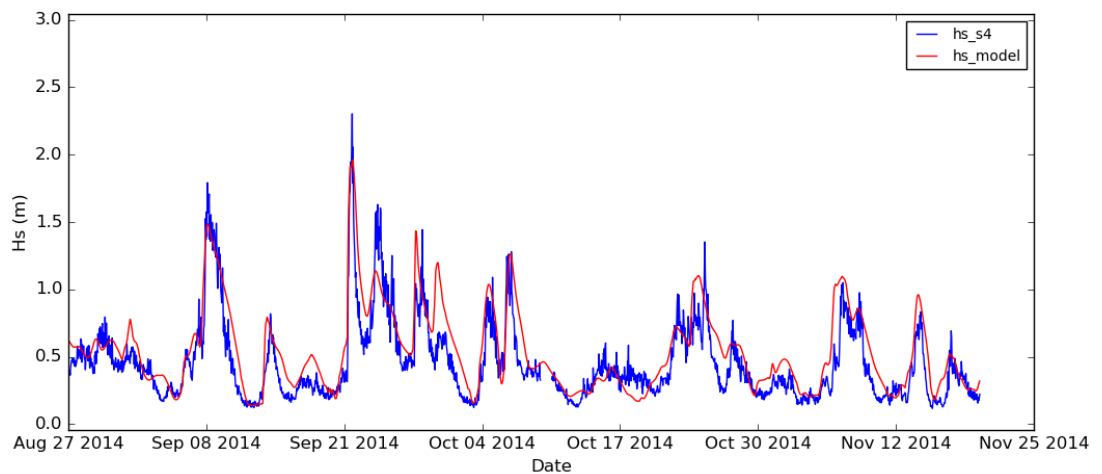


Figure 3.11. Time series of measured and modelled significant wave height  $H_s$  at site WB1 during 2014.

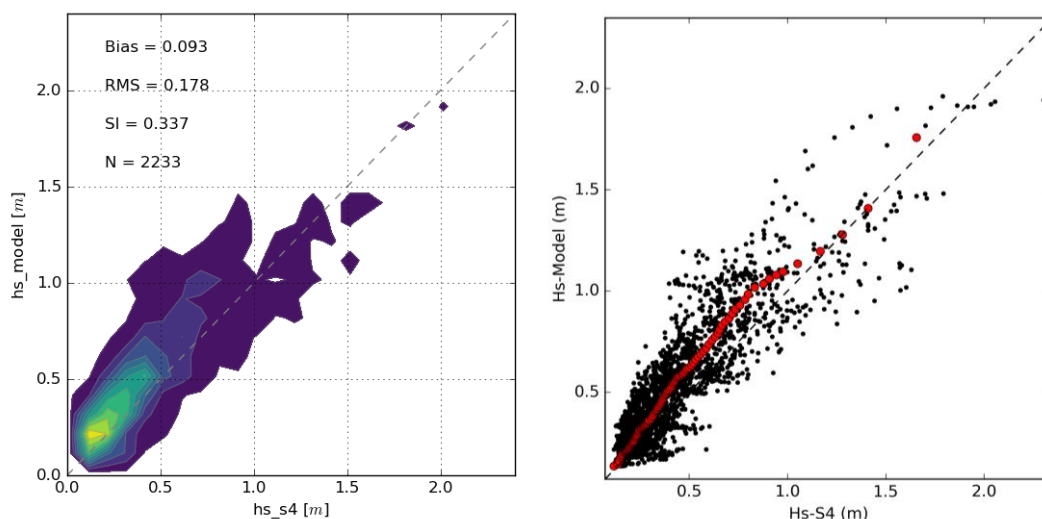


Figure 3.12. Scatter density (left) and scatter diagram (right) comparing measured and modelled significant wave height  $H_s$  at A1 site for 2014. Hot colours on the left indicate higher density of data-points. Red circles on the right show the quantile-quantile at the 0.01 percentile.

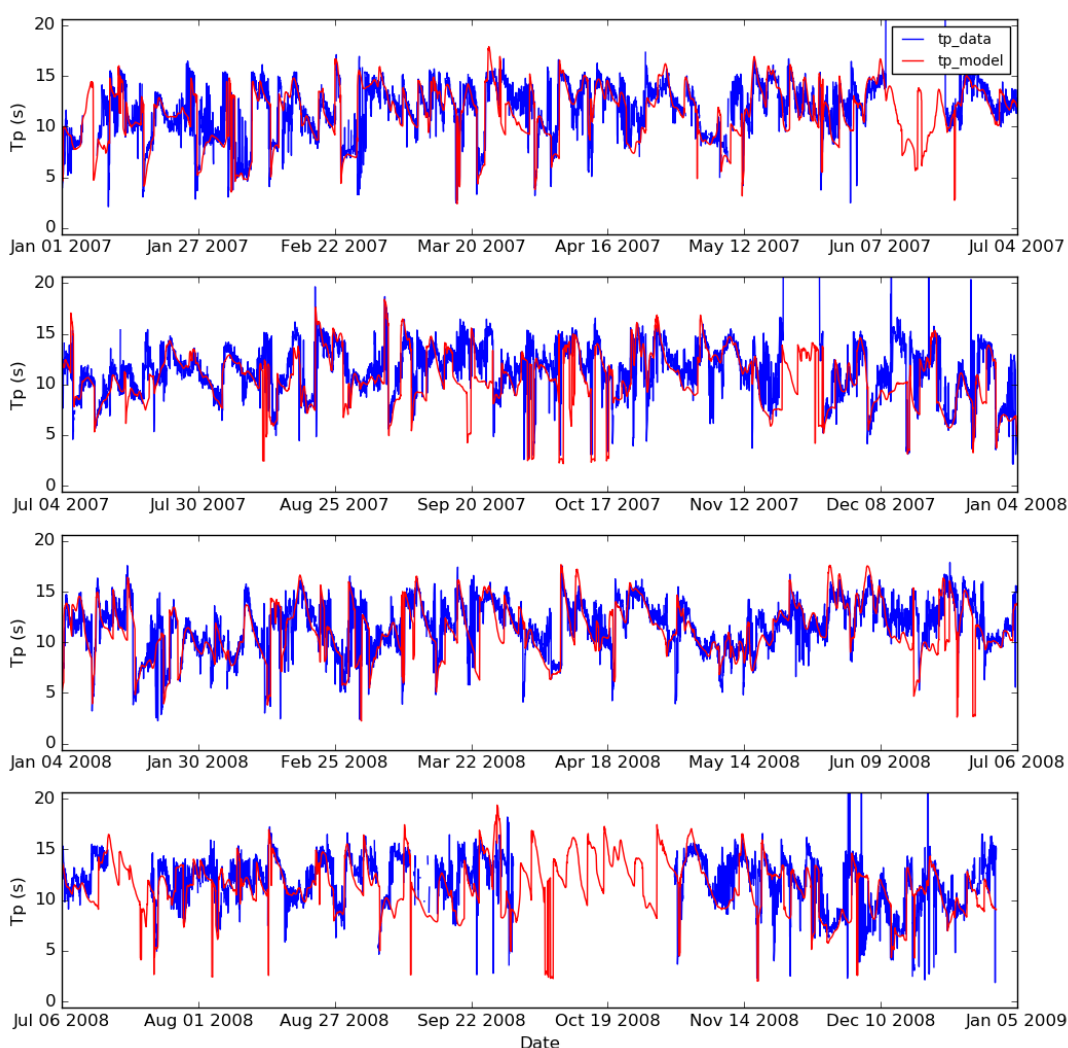


Figure 3.13. Time series of measured and modelled peak wave period  $T_p$  at site WB1 between 2007 – 2008.

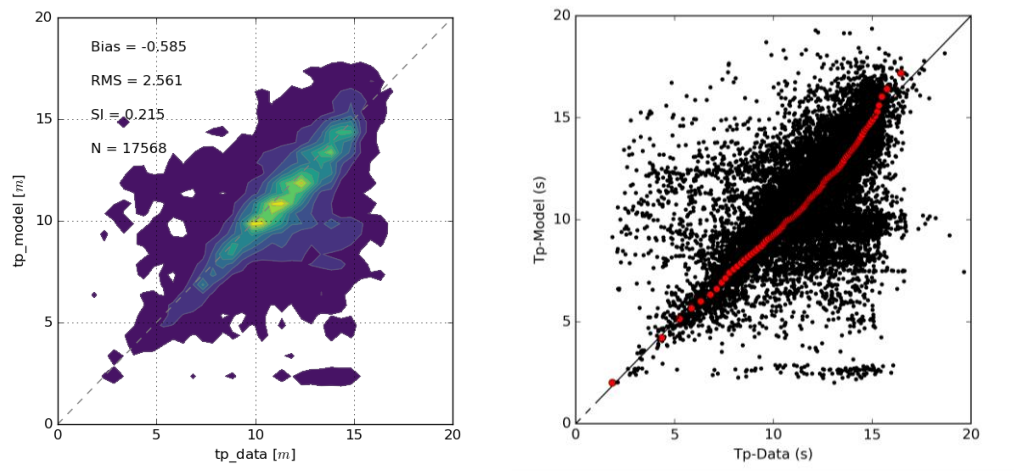


Figure 3.14. Scatter density (left) and scatter diagram (right) comparing measured and modelled peak wave period  $T_p$  at WB1 site for years 2007–2008. Hot colours on the left indicate higher density of data-points. Red circles on the right show the quantile-quantile at the 0.01 percentile.

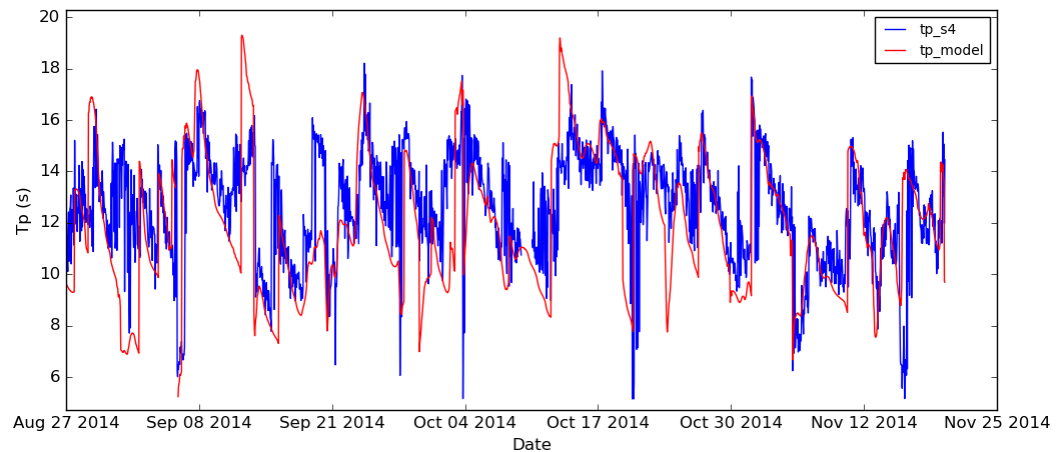


Figure 3.15. Time series of measured and modelled peak wave period  $T_p$  at site A1 during 2014.

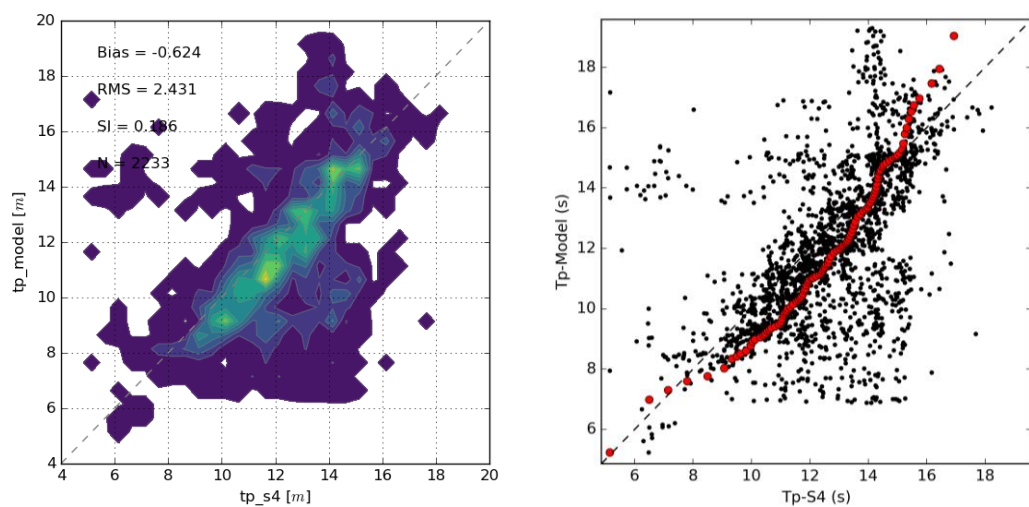


Figure 3.16. Scatter density (left) and scatter diagram (right) comparing measured and modelled significant peak wave period  $T_p$  at A1 site during 2014. Hot colours on the left indicate higher density of data-points. Red circles on the right show the quantile-quantile at the 0.01 percentile.

### 3.1.3. Bias-corrected significant wave height

Model significant wave height fields were bias-corrected using time series of significant wave height recorded by the wave buoy deployed at Site WB1 between 2007 and 2008. Accuracy measured for both original and bias-corrected significant wave heights at positions WB1 and A1 are summarised in Table 3.3.

Time series of measured and bias-corrected modelled significant wave heights are presented in Figure 3.17 and Figure 3.19. Scatter density plots and diagrams comparing measured and bias-corrected modelled significant wave heights are shown in Figure 3.18 and Figure 3.20.

Accuracy statistics were considerably improved at position WB1 after applying the polynomial correction. Pre- and post-correction biases were -0.10 and 0.00 m while scatter indexes were 0.24 and 0.23, respectively. These accuracy measures highlighted the good agreement between measured and hindcast  $H_s$ . The peak  $H_s$  for three large events around 09<sup>th</sup>, 22<sup>nd</sup> and 25<sup>th</sup> September 2014 were notably closer in the corrected model.

At position A1, the bias correction had little effect since  $H_s$  was substantially smaller (mean  $H_s$  during the 85 days of 0.45 m) than at position WB1 due to sheltering and dissipative effects over the adjacent reefs.

More broadly, the overall model performance assessment showed satisfactory results making the wave model suitable for forcing the subsequent morphological models.

Table 3.3 Comparison between measured and (bias-corrected) hindcast wave data. Accuracy measures for significant wave height ( $H_s$ ) at sites WB1 and A1.

Sites	Parameters	Bias	RMSE	MAE	MRAE	Scatter Index
WB1	$H_s$ [m]	-0.10	0.26	0.18	0.18	0.24
	$H_s$ corrected [m]	0.00	0.24	0.17	0.19	0.23
A1	$H_s$ [m]	0.09	0.18	0.14	0.36	0.34
	$H_s$ corrected [m]	0.10	0.19	0.14	0.37	0.34

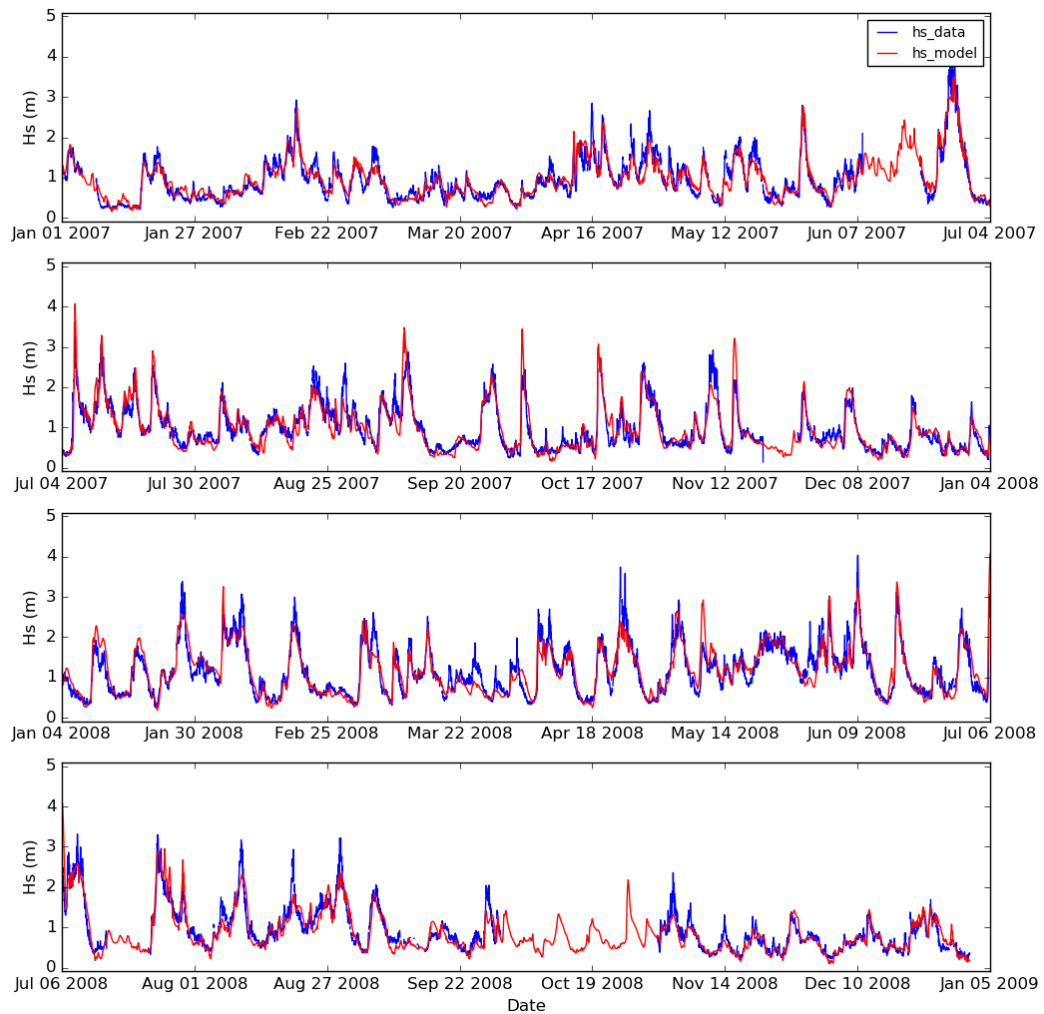


Figure 3.17. Time series of measured and bias-corrected, modelled significant wave height  $H_s$  at site WB1 between 2007 – 2008.

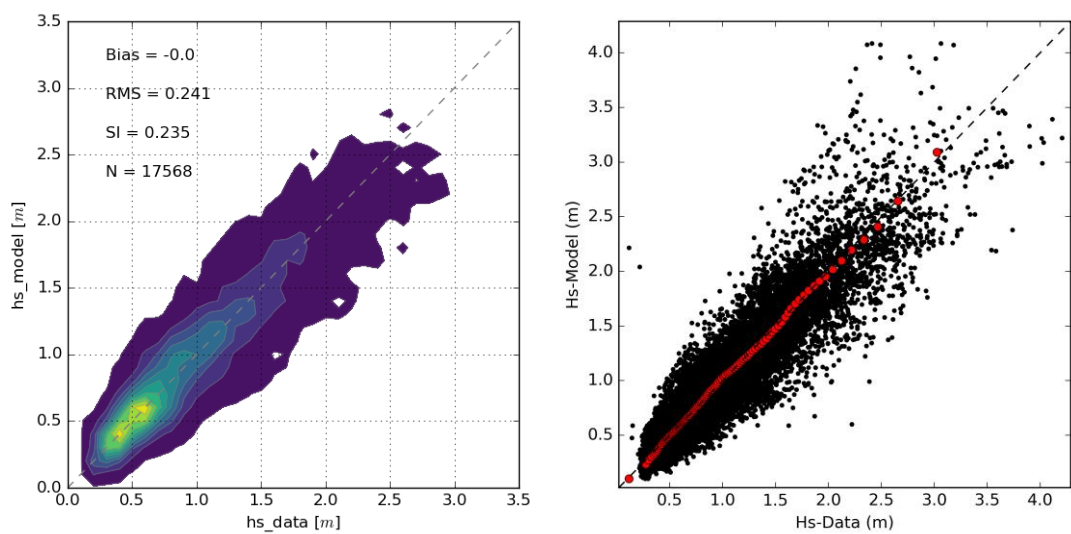


Figure 3.18. Scatter density (left) and scatter diagram (right) comparing measured and bias-corrected, modelled significant wave height  $H_s$  at WB1 site for years 2007–2008. Hot

colours on the left indicate higher density of data-points. Red circles on the right show the quantile-quantile at the 0.01 percentile.

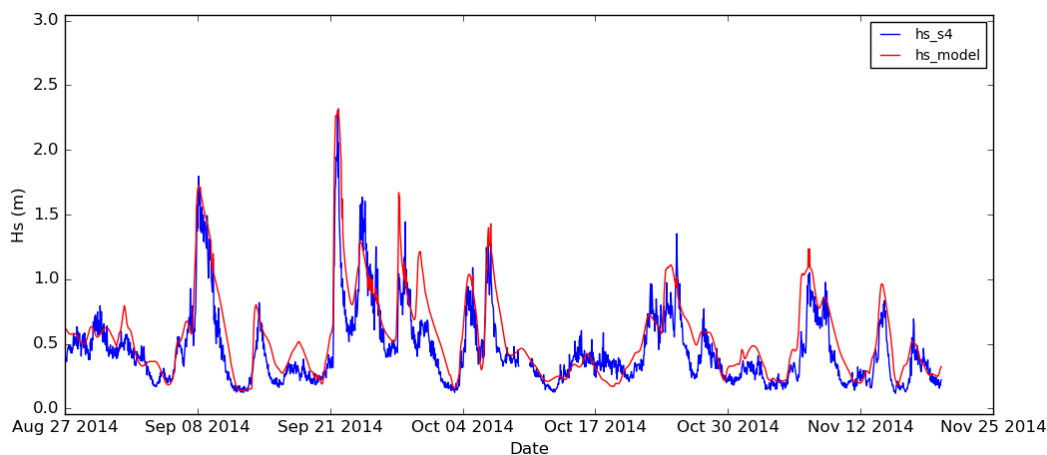


Figure 3.19. Time series of measured and bias-corrected, modelled significant wave  $H_s$  height at site A1 during 2014.

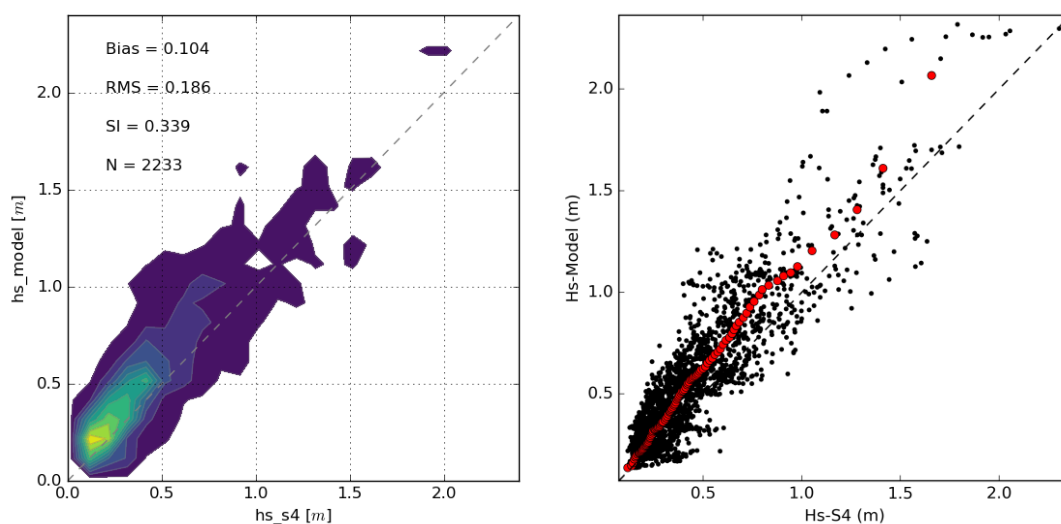


Figure 3.20. Scatter density (left) and scatter diagram (right) comparing measured and bias-corrected, modelled significant wave height  $H_s$  at A1 site for 2014. Hot colours on the left indicate higher density of data-points. Red circles on the right show the quantile-quantile at the 0.01 percentile.

### 3.2. Wave climate

Examples of the spatial distribution in wave height within each of the nested SWAN domains for a significant southerly storm on the 29<sup>th</sup> July 2012 are shown in Figure 3.21, Figure 3.22 and Figure 3.23.

Within the NZN domain, significant wave heights approaching 8-m are expected offshore on the 29<sup>th</sup> July 2012. Larger scale features such as Cape Kidnappers and Mahia Peninsula are shown to effect the propagation of wave energy into the coastal and nearshore regions of Hawke Bay and north of Mahia Peninsular, including Poverty Bay respectively (Figure 3.21).

For this particular event, the topographical shadowing of Mahia Peninsular is clearly shown in Figure 3.22, with wave heights attenuated significantly within Poverty Bay. The spatial distribution of wave heights within the Poverty Bay and Eastland SWAN domains show a relatively complex distribution due to the offshore reef systems and wave shadowing behind Young Nicks Head (Figure 3.23). Additionally, the SWAN modelling clearly shows the wave height enhancement and focusing due to Tokomaru, Hawea and Temoana Rocks (Figure 3.23), with slightly larger wave heights expected along parts of Waikanea Beach consistent with the locations of the predominant Surf spots within Poverty Bay (Pipe and Roberts Road).

The 10-year (bias-corrected) hindcast data at Sites WB1 and A1 were used to characterise the nearshore wave climate (see wave statistics in Table 3.4 and Table 3.5). Box plots and wave rose diagrams extracted from the time series of significant wave height and peak wave direction at both positions are provided in Figure 3.24 and Figure 3.25. Results of the extreme wave analysis carried out at Sites WB1 and A1 from the 10-year hindcast time series of significant wave height and peak wave period are presented in Figure 3.26 and Figure 3.27, and in Table 3.6.

The dissipative effects caused by bottom friction at Tokomaru, Hawea and Temoana Rocks and near the entrance to Eastland Port contribute to attenuate significantly the wave energy over the northern area of Poverty Bay. The significant wave height values are typically reduced by a factor 1.5 – 2 between WB1 and A1. The 100-year return period value significant wave height does not exceed 3.5 m at Site A1 against 6.7 m at Site WB1. In the meantime, the topography over the navigation channel induces a shift in the wave direction from SE to S by refraction.

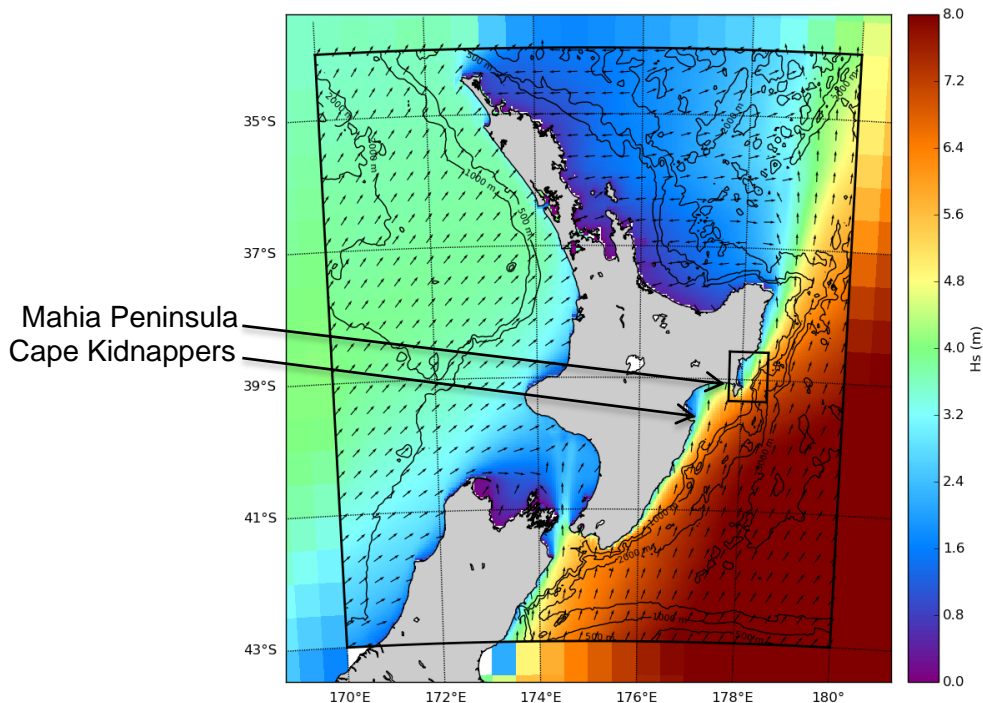


Figure 3.21. Snapshot of significant wave height from the NZN 4 km SWAN parent domain on 29 July 2012, shown within the area delimited by the outer black rectangle. Model data from the 0.5° global wave model are shown outside of this area. Extension of Gisborne child nest is shown by the inner black rectangle.

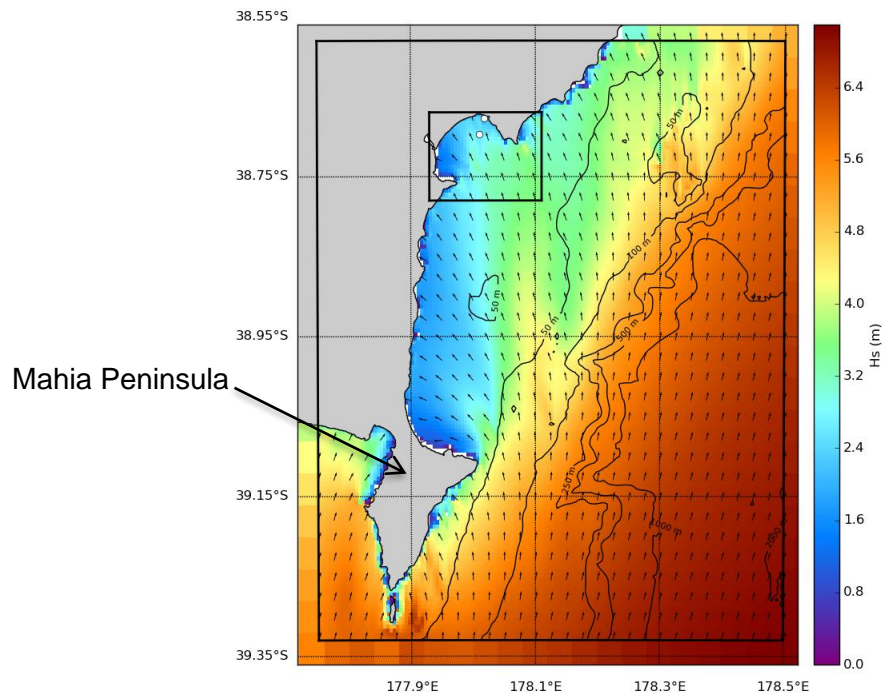


Figure 3.22. Snapshot of significant wave height from the Gisborne 500 m SWAN child domain on 29 July 2012, shown within the area delimited by the outer black rectangle. Model data from the 4 km NZN domain are shown outside of this area. Extension of Poverty Bay child nest is shown by the inner black rectangle.

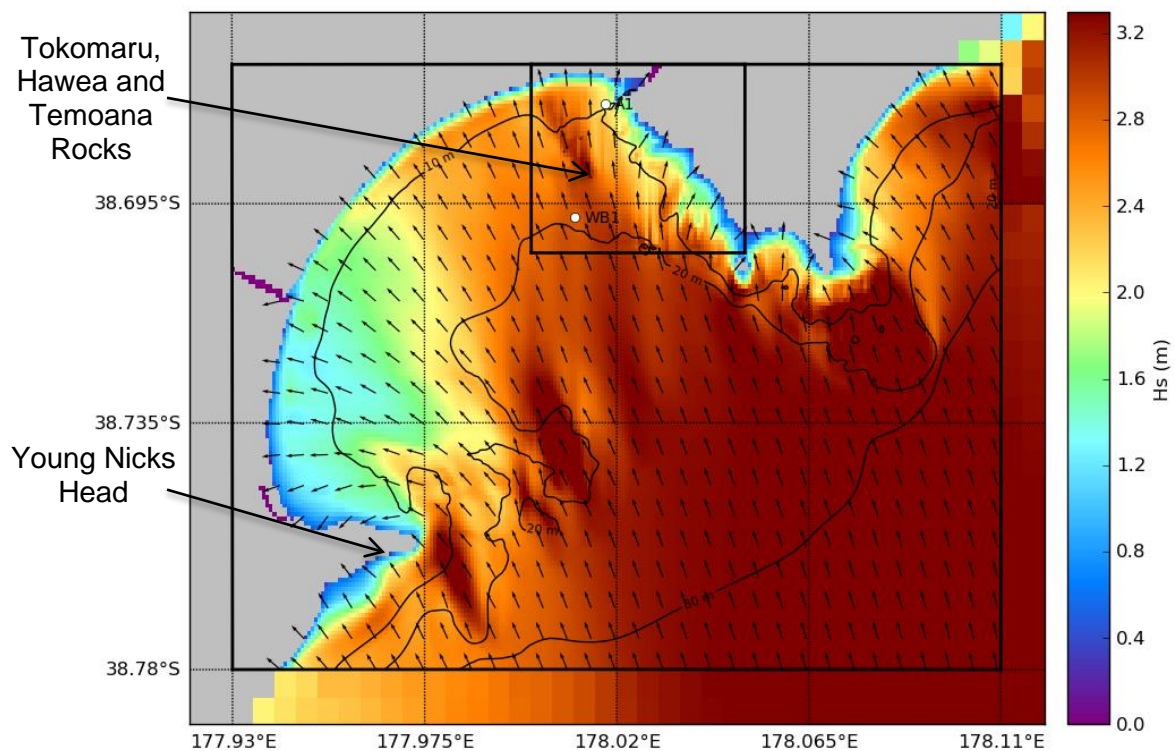


Figure 3.23. Snapshot of significant wave height from the Poverty Bay 80 m SWAN child domain on 29 July 2012, shown within the area delimited by the outer black rectangle. Model data from the 500 m Gisborne domain are shown outside of this area. Extension of Eastland child nest is shown by the inner black rectangle.

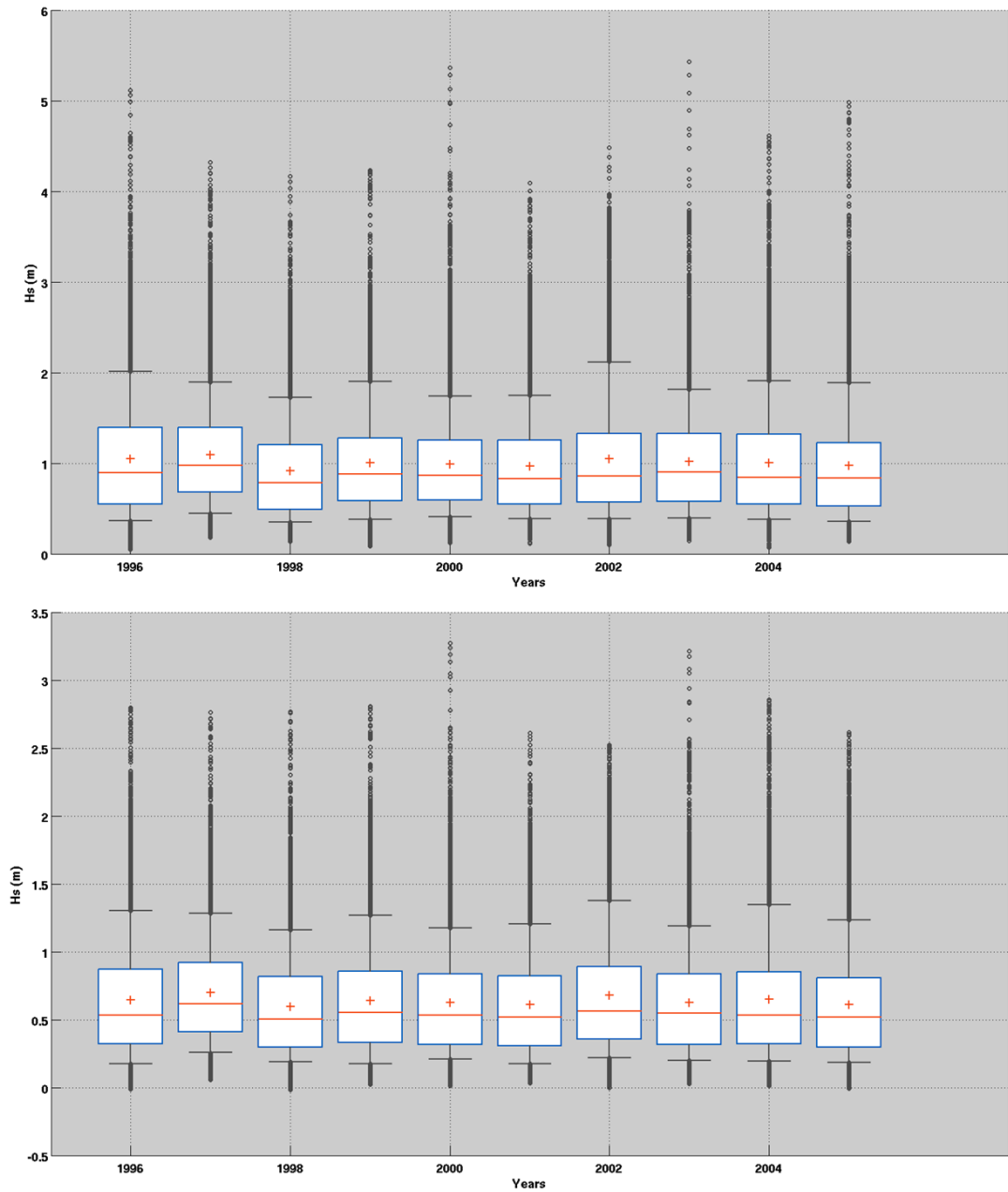


Figure 3.24. Boxplots extracted from time series of significant wave height at Sites WB1 (top) and A1 (bottom). The blue rectangles correspond to the 25<sup>th</sup> – 75<sup>th</sup> percentiles of the annual distributions. Red crosses and red lines indicate the annual median and mean, respectively. The grey dots correspond to the outliers based on the 95<sup>th</sup> percentile threshold.

Table 3.4 Total and monthly significant wave height statistics at Site WB1 based on 10 year hindcast (1996 – 2005).

Statistics Site WB1	min	max	mean	std	p50	p90	p95	p99	Main direction
January	0.13	4.03	0.85	0.55	0.70	1.55	1.97	2.84	SE S
February	0.13	3.79	0.86	0.52	0.73	1.53	1.86	2.65	SE S
March	0.10	5.11	0.96	0.56	0.84	1.70	2.01	2.93	SE S
April	0.16	3.75	1.08	0.58	0.97	1.92	2.24	2.91	SE S
May	0.21	4.23	1.07	0.58	0.94	1.80	2.15	3.01	SE S
June	0.07	4.60	1.21	0.69	1.06	2.10	2.46	3.63	SE S
July	0.17	5.43	1.29	0.65	1.18	2.17	2.45	3.20	SE S
August	0.19	4.61	1.22	0.63	1.08	2.14	2.45	3.09	SE
September	0.14	5.37	0.98	0.60	0.83	1.78	2.10	2.80	SE S
October	0.09	4.09	0.89	0.55	0.74	1.61	2.02	2.74	SE S
November	0.11	4.98	0.91	0.55	0.77	1.58	1.87	2.69	SE S
December	0.04	2.68	0.73	0.40	0.64	1.27	1.54	2.00	SE S
Summer	0.04	5.11	0.87	0.53	0.73	1.55	1.90	2.67	SE S
Winter	0.07	5.43	1.14	0.63	1.02	2.00	2.33	3.14	SE S
<b>Total</b>	<b>0.04</b>	<b>5.43</b>	<b>1.00</b>	<b>0.60</b>	<b>0.87</b>	<b>1.81</b>	<b>2.16</b>	<b>2.96</b>	<b>SE S</b>

Table 3.5 Total and monthly significant wave height statistics at Site A1 based on 10 year hindcast (1996 – 2005).

Statistics Site A1	Min	Max	Mean	Std	P50	P90	P95	P99	Main direction
January	0.03	2.68	0.52	0.37	0.43	1.02	1.25	1.83	S
February	0.02	2.52	0.54	0.35	0.47	0.99	1.22	1.83	S
March	-0.00	2.69	0.60	0.37	0.52	1.11	1.38	1.87	S
April	0.05	2.28	0.71	0.41	0.63	1.29	1.53	1.97	S
May	0.07	2.81	0.69	0.42	0.60	1.24	1.47	2.09	S
June	0.02	2.79	0.78	0.49	0.68	1.42	1.68	2.43	S
July	0.01	3.22	0.78	0.44	0.72	1.41	1.58	1.97	S
August	0.06	2.86	0.74	0.45	0.63	1.40	1.62	2.11	S
September	-0.01	3.27	0.62	0.44	0.52	1.23	1.45	1.92	S
October	0.04	2.61	0.59	0.39	0.50	1.14	1.42	1.85	S
November	0.01	2.62	0.60	0.39	0.51	1.10	1.35	1.91	S
December	-0.02	2.06	0.47	0.32	0.40	0.92	1.12	1.46	S
Summer	-0.02	2.69	0.55	0.37	0.47	1.05	1.29	1.82	S
Winter	-0.01	3.27	0.72	0.44	0.64	1.34	1.57	2.09	S
<b>Total</b>	<b>-0.02</b>	<b>3.27</b>	<b>0.64</b>	<b>0.42</b>	<b>0.54</b>	<b>1.21</b>	<b>1.46</b>	<b>1.97</b>	<b>S</b>

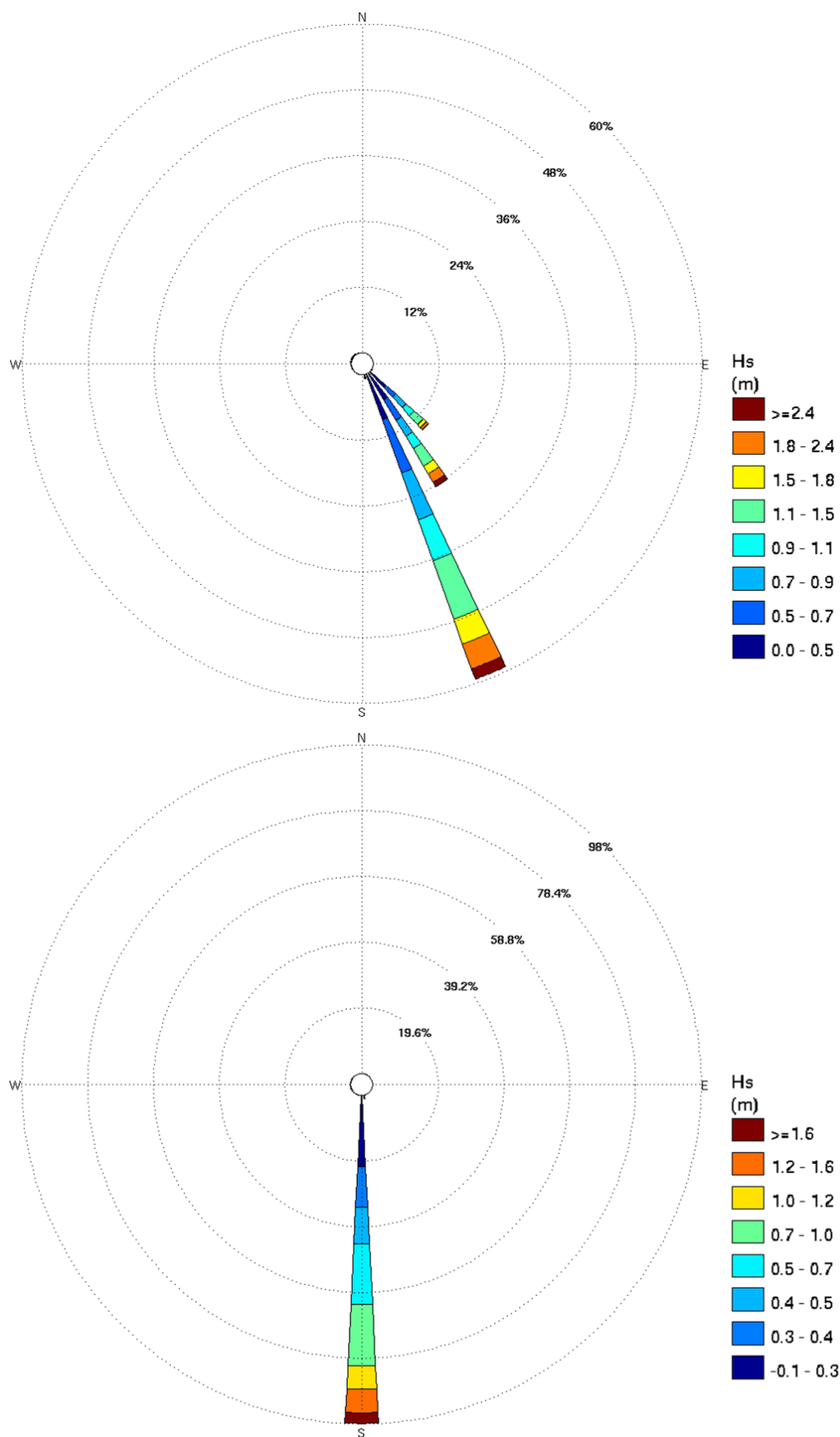


Figure 3.25. Wave rose diagrams based on 10 year hindcast data (1996 – 2005) at Sites WB1 (top) and A1 (bottom). The direction follows the nautical “coming from” convention.

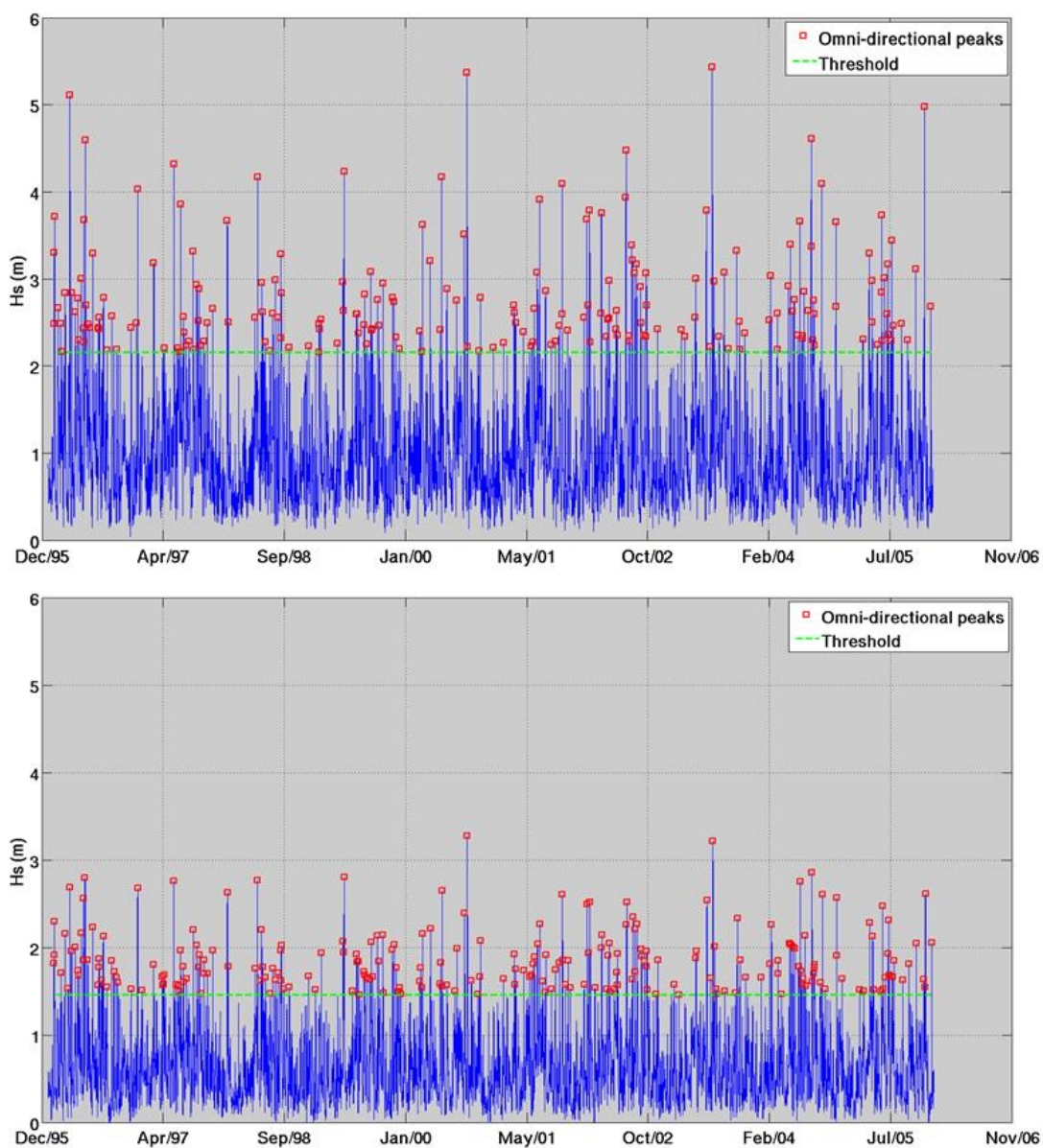


Figure 3.26. Significant wave height ( $H_s$ ) time series at Sites WB1 (top) and A1 (bottom) including the extreme events detected from the Peaks over Threshold (POT) methodology. The dashed green line indicates the minimum threshold used for the detection of extreme events corresponding to the 95<sup>th</sup> percentile level of the distribution.

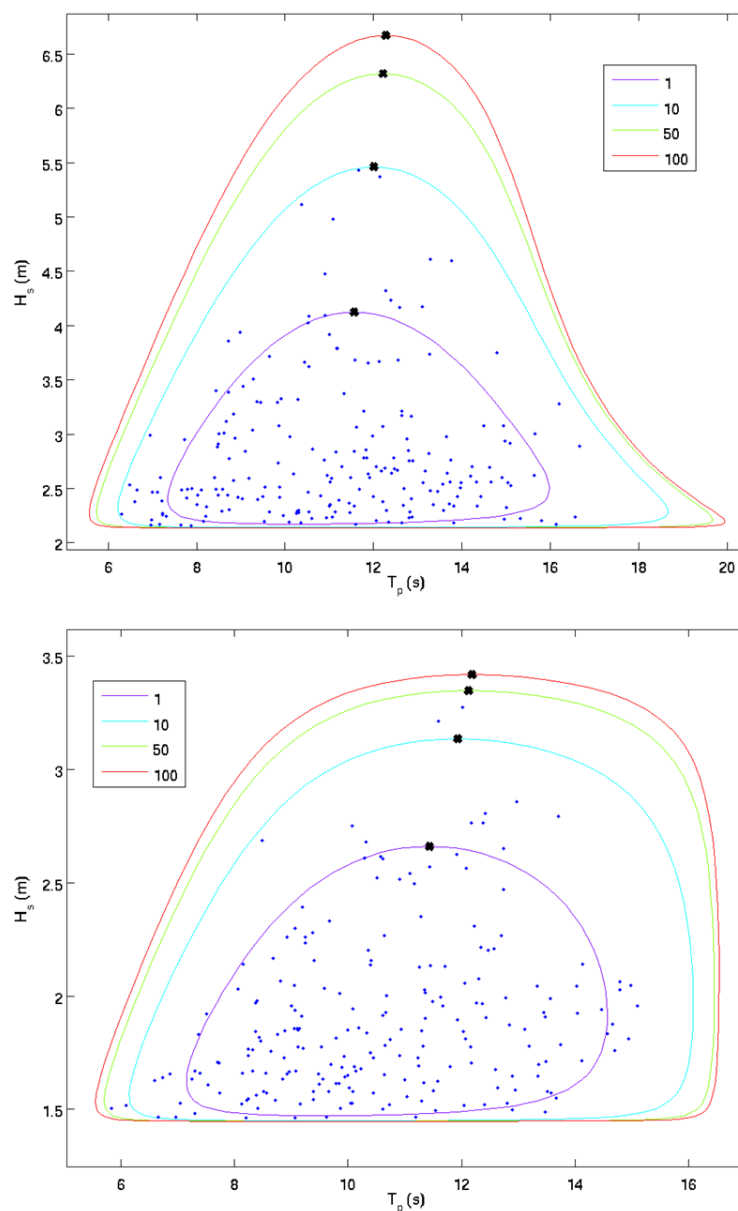


Figure 3.27. Contour plot of omnidirectional bi-variate return period values for 1, 10, 50 and 100 year ARIs for significant wave height and peak wave period at Sites WB1 (top) and A1 (bottom). The dark crosses correspond to the estimated deterministic  $H_s$  and associated  $T_p$  return period values for each ARI (years) indicated in this legend.

Table 3.6 Omnidirectional  $H_s$  and associated  $T_p$  return period values for 1, 10, 50 and 100 year ARIs using the 10 year hindcast data at Sites WB1 and A1.

ARI (years)	Site (WB1)		Site (A1)	
	$H_s$ (m)	$T_p$ (s)	$H_s$ (m)	$T_p$ (s)
1	4.122	11.561	2.661	11.433
10	5.461	12.008	3.137	11.93
50	6.32	12.211	3.349	12.123
100	6.672	12.281	3.419	12.183

## **4. SUMMARY**

The open-source SWAN model was used to hindcast the wave climate within Poverty Bay and at the entrance to Eastland Port over ten years. A four-level nesting approach was employed to simulate the spectral wave transformation to the coastal region.

The model was validated with measurements from two locations, and was shown to under-predict some of the extreme wave events partly due to limitations in the global model. In order to minimise some of this low-bias, a bias correction technique was successfully applied based on measured and modelled time series of significant wave height at one site located in Poverty Bay. Wave statistics based on the bias-corrected wave hindcast were provided. The bias-corrected SWAN model achieved good nearshore correlation at the port entrance making this tool appropriate to force the subsequent morphological and plume models.

## 5. REFERENCES

- Ardhuin, F., Rogers, E., Babanin, A.V., Filipot, J.F., Magne, R., Roland, A., Van Der Westhuysen, A., Queffelec, P., Lefevre, J., Aouf, L., Collard, F., 2010. Semiempirical dissipation source functions for ocean waves. Part I: Definition, calibration, and validation. *J. Phys. Oceanogr.* 40, 1917–1941.
- Chappell, P.R., 2016. The climate and weather of Gisborne (No. ISSN 1173-0382). NIWA.
- Collins, J., 1972. Prediction of Shallow Water Spectra. *J. Geophys. Res.* 77, 2693–2707.
- Holthuijsen, L.H., Booij, N., Ris, R.C., Haagsma, I.J., Kieftenburg, A.T.M.M., Kriezi, E.E., Zijlema, M., van der Westhuysen, A.J., 2007. SWAN cycle III version 40.51, Technical Documentation. Delft, 2600 GA Delft The Netherlands.
- Tolman, H.L., 1991. A Third-Generation Model for Wind Waves on Slowly Varying, Unsteady and Inhomogeneous Depths and Currents. *J. Phys. Oceanogr.* 21, 782–797.
- Van der Westhuysen, A.J., Zijlema, M., Battjes, J.A., 2007. Nonlinear saturation-based whitecapping dissipation in SWAN for deep and shallow water. *Coast. Eng.* 54, 151–170. doi:10.1016/j.coastaleng.2006.08.006

## APPENDIX A. MEASURED AND HINDCAST WIND ROSES AT HICKS BAY

### Hicks Bay [178.314 E; 37.564 S]

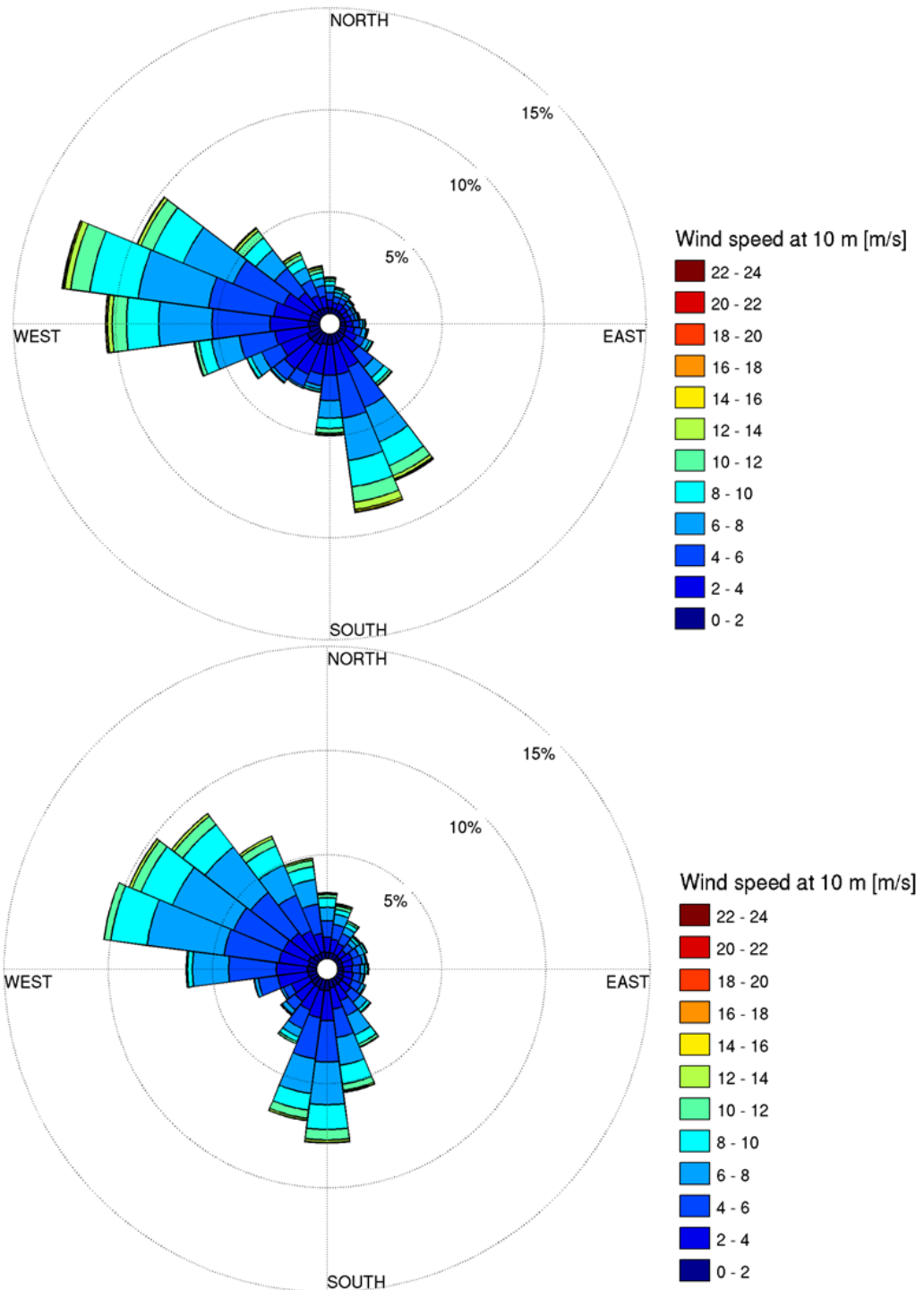


Figure A.1 Measured and hindcast wind rose at 10 m extracted at Hicks Bay between 2000 and 2008.